SHOCK REFLECTION AND INTERACTION AT HYPERSONIC SPEEDS

by

S. Molder and E.J. Szpiro

Report No. 63-8

Hypersonic and Propulsion Laboratory

Mechanical Engineering Research Laboratories

McGill University

Supported under D.R.B. Grant Number 9550-06

Montreal May, 1963.

SUMMARY

This report presents the calculated thermodynamic and oblique shock data for hypersonic double oblique shock waves. Work was done for a real gas (air) along a room number altitude path which is representative of possible hypersonic cruise flight capabilities. Results are given for the dynamic and thermodynamic variables during and after the shock interaction, and also for the geometry of the interaction. Results are calculated for various wedge angles and Mach numbers. A detailed examination of the effect of angles of attack is included. Throughout, special emphasis is placed on conditions which are thought to be suitable for the use of the double oblique shock system as an inlet for hypersonic engines.

In general, this type of inlet is found to be relatively insensitive to variations in Mach number and angle of attack.

SUMMARY

This report presents the calculated thermodynamic and oblique shock data for hypersonic double oblique shock waves. This was done for a real gas (air) along a Mach number-altitude relationship representative of possible hypersonic ramjet flight capabilities. Results are given for the dynamic and thermodynamic variables during and after the shock interaction, and also for the geometry of the interaction. Results are calculated for various wedge angles and Mach numbers. A detailed examination of the effect of angles of attack is included. Throughout, special emphasis is placed on conditions which are thought to be suitable for the use of the double oblique shock system as an intake for hypersonic ramjets.

In general, this type of intake is found to be relatively insensitive to variations in Mach number and angle of attack .

ACKNOWLEDGEMENTS

We are indebted to Mr. A.M. Valenti for reading and correcting the manuscript.

Thanks are also extended to Miss J. Fitzpatrick who typed this report, to Mr. M. Merilo for drawing several graphs and to the McGill University Computing Centre for their assistance in programming.

The financial support of the Defence Research Board of Canada is also acknowledged.

TABLE OF CONTENTS

1. NOTATION

a	fps	speed of sound
d	deg.	geometrical wedge angle
h	Btu/lb.	static enthalpy
H	ft.,m.	geopotential altitude
M	--	Mach number
p	psf	static pressure
S	Btu/lb.-°K	entropy
T	°K	temperature
u	fps	velocity component normal to shock
v	fps	velocity component parallel to shock
V	fps	velocity (absolute component)
Z	--	compressibility factor
α	deg.	angle of attack
γ	--	specific heat ratio (C_p/C_v)
δ	deg.	aerodynamic flow deflection angle w.r.t. free stream direction
ϵ	deg.	contact surface deflection angle w.r.t. free stream direction
θ	deg.	shock wave angle
ρ	pcf	density

Subscripts

∞	initial free stream flow conditions
1,2	variables for regions 1 and 2 respectively, aft of the first shocks, as shown in Fig. 3
3,4,	variables for regions 3 and 4 respectively, aft of the reflected shocks, as shown in Fig. 3
x	parameters in front of a shock
y	parameters aft of a shock

2. INTRODUCTION

Mach showed in 1878 (Ref. 1) that if in an inviscid supersonic stream a shock wave is made to impinge on a plane wall then two flow geometries are possible. The first possibility is one for which the approaching flow is made to turn towards the wall by the incident shock and then this flow is turned back by the reflected shock to the freestream direction. This type of reflection is called regular reflection. For the other configuration the incident shock must be stronger than it was for the regular interaction. The flow is now turned more sharply towards the wall, and if the deflection required to bring it back to the freestream direction is larger than a given critical angle (Ref. 2) then the reflected shock will tend to detach. However, detachment cannot take place because of the incident shock's presence. Instead a three-shock configuration of the following general shape presents itself: a normal shock extends some distance up from the surface at which point it divides into an incident and reflected shock. The flow behind the normal shock is subsonic and behind the reflected shock it is supersonic. These two flow regions are separated by a shear layer emanating from the intersection of the three shocks. This type of reflection is usually referred to as irregular or Mach reflection.

For inviscid flow, the plane wall may be considered to be a stream line of symmetry in which case a mirror image of either of the above types of reflections may be thought of as occurring below this line. In this case the shocks are interacting instead of reflecting and as for reflections,

there exist two possible flow geometries called regular interaction and Mach interaction. Figures 1 and 2 depict regular and Mach interaction in a Mach 2.48 stream (Ref. 3).

Experimental studies of shock reflections from a plane wall have been performed with a moving shock in a shock tube by Smith (Ref. 4). Corresponding work has been done in steady flow in a super-sonic wind tunnel (Refs. 3, 5, 6). These show satisfactory agreement with theory for regular interactions. There has been no experimental work on shock reflections or interactions for hypersonic flows; this includes both regular and Mach configurations. No theoretical calculations have been published of regular or Mach interactions in hypersonic flow.

This Report contains calculations of the interaction of plane oblique shock waves at hypersonic speeds. A real gas (Mollier chart) is assumed. The calculations are limited to regular interactions for a Mach number range of 8 to 30. Free stream conditions are limited to an altitude - Mach number relationship appropriate to boosting of satellite vehicles by hypersonic ramjet booster stages.

3. PRELIMINARY CONSIDERATIONS

3.1 Shock Reflection

Figure A shows the reflection of a shock from a straight wall. Since the gas flow is assumed to follow the solid boundary, it is necessary for shock B to be reflected so that the stream in region 3 will have the same direction as in region 1. Shocks A and B turn the flow through equal angles δ. It is thus evident that an oblique shock is reflected from a solid wall as another oblique shock (Ref. 7). It can be shown that for a given value of the stream Mach number, there is a maximum value of turning angle (δ_{max}) beyond which regular reflection is not possible and Mach reflection takes place.

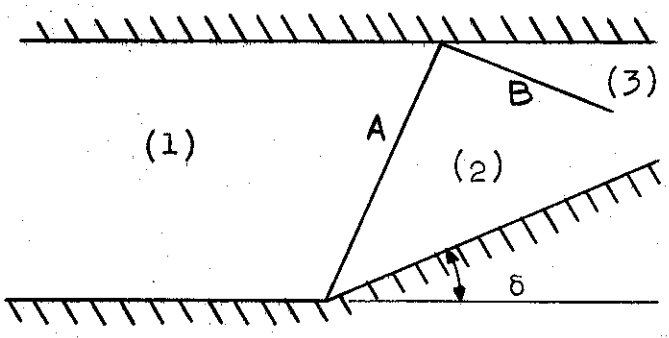

Fig. A Shock Reflection from a Solid Wall

3.2 Shock Interaction

The foregoing description of shock reflection applies with a few modifications to shock interaction.

Figure B illustrates regular interaction produced by two equal shocks, originating from oppositely placed wedges. The flow is symmetrical about the plane ABC, and thus the plane ABC may be replaced by a wall. The shocks may now be considered to be reflecting instead of interacting at point B. An important difference between the reflection of shock waves from walls and the interaction of equal or unequal shock waves is that the latter is free from the viscous effects of boundary layer at the point of reflection or interaction.

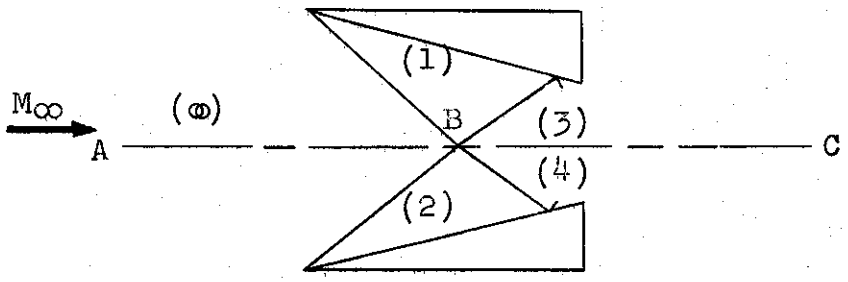

Fig. B Interaction of Two Equal Oblique Shocks

However, if the incident shocks are not of equal strength the picture is no longer symmetrical and consideration must be given to both sides of ABX (Fig. C).

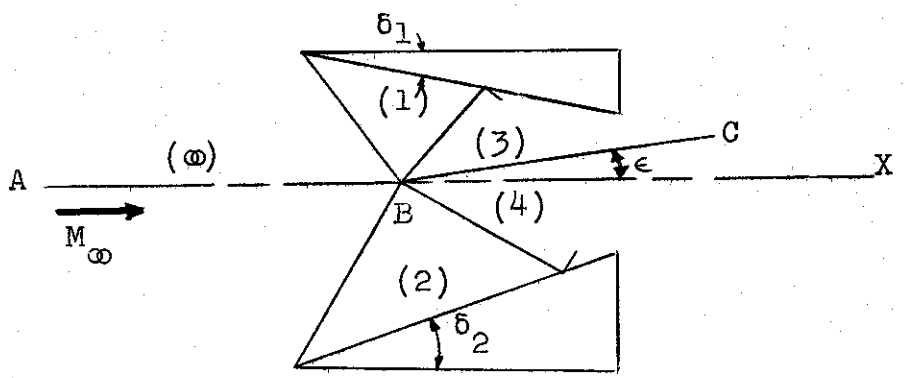

Fig. C Interaction of Two Unequal Oblique Shocks

Thus, ABC is no longer a plane of symmetry, since BC is inclined to AB at an angle ϵ. This angle (ϵ) represents the deflection of the initial free stream flow as it passes through the shocks. The line BC separates two uniform regions of air which have undergone compressions through two different shock systems. The flow direction and static pressure above and below BC are the same; while the Mach number, velocity, and density are different. The discontinuity in the flow speed across BC gives rise to a high vorticity layer known as a vortex sheet or a slip plane.

The interaction of unequal shocks may still be treated as a reflection problem, the only difference being that at the point of reflection (or interaction) the wall (in this case the streamline through the interaction point) is deflected towards or away from the upstream flow.

3.3 Wedge Representations

If the equal wedges shown in Fig. B are rotated by an angle α with respect to the free stream flow direction, then the flow is deflected by unequal amounts by the two wedges. Geometry as shown in Fig. D results. This is equivalent to having no flow deflection angle, α, with the wedge angles (d) now replaced by effective aerodynamic angles δ_1 and δ_2 (Fig. C). The angle α is referred to as the angle of attack. The angle of attack is considered positive when the intake nose is pointed downwards. This is in opposition to the conventional definition of angle of attack.

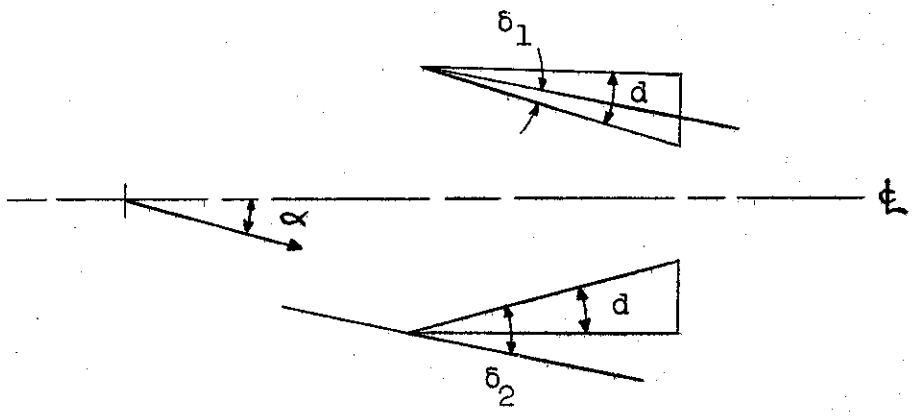

Fig. D Physical Representation of Inlets

From Fig. D , it is seen that:

$$\delta_1 = d - \alpha \tag{1}$$

$$\delta_2 = d + \alpha \tag{2}$$

Thus,

$$\alpha = \frac{\delta_2 - \delta_1}{2} \tag{3}$$

$$d = \frac{\delta_1 + \delta_2}{2} \tag{4}$$

3.4 Free Stream Conditions and a Flight Corridor

The flight corridor, as described in Ref. 8 , is shown in Fig. 4 . The curve labeled HIGH ALTITUDE OF CRUISE VEHICLES is reached when not enough dynamic pressure and centrifugal lift exist to balance the weight of winged hypersonic vehicles. The curve labeled LOW ALTITUDE THERMAL LIMIT OF SPACE BOOSTERS is determined by the cooling capabilities of the aircraft. Relatively long flight times are permissible in the vicinity of the thermal limit. The region between the high altitude limit and the thermal limit is the FLIGHT CORRIDOR.

The free stream conditions are calculated from a given free stream Mach number, since the BOOST (Low Altitude Thermal Limit of Space Boosters) curve defines a Mach number - Altitude relationship. The free stream pressure and temperature are then calculated for the different altitudes with the equations listed in Appendix C . Using $\gamma = 1.4$ and $Z = 1$ (Ref. 9), the other free stream parameters (h_∞, ρ_∞, α_∞, S_∞, V_∞) are calculated using the equations of Sect. 6.2.

4. OBLIQUE SHOCKS IN HYPERSONIC FLOW

One method for determining two-dimensional oblique shock characteristics in hypersonic flow is presented below. This method is substantially the same as that of Reference 10, with one basic difference. This is that while the method of Reference 10 uses two iterations, the one described herein rearranges the equation so as to use only one iteration.

The basic assumptions and some of their implications are presented below:

1. Aerodynamics of continuum flow apply. This assumption implies that the mean free path of the molecules is short enough to result in a small physical thickness of the shock as compared with the characteristic length of the object causing the shock. This generally holds true for altitudes less than 300,000 ft., but deviations occur as altitudes above this are reached. A further discussion of continuum flow assumptions with respect to intakes is given in Reference 8.
2. Thermal and chemical equilibrium exists aft of the shock wave. This assumption applies after whatever distance is required to achieve equilibrium among the various energy states including vibration, dissociation and ionization. Although the distance required for complete equilibrium is greater than the physical shock thickness, equilibrium may be assumed in all practical cases below an altitude of 300,000 ft. A discussion of equilibrium flow with respect to hypersonic intakes is given in Reference 8.

3. The atmospheric properties of Reference 9 exist in front of the shock wave.
4. The argon-free air properties (including real gas effects) exist aft of the shock wave.
5. The oblique shock is straight and is attached to the leading edge of a two dimensional flat surface (cowl).
6. The velocity component parallel to the shock wave, remains unchanged in passing through the shock and therefore has no effect on the properties aft of the shock wave.
7. The properties aft of the shock exist outside of the boundary layer and are unaffected by interaction with the boundary layer.

The following diagram illustrates the geometry of a two-dimensional attached shock:

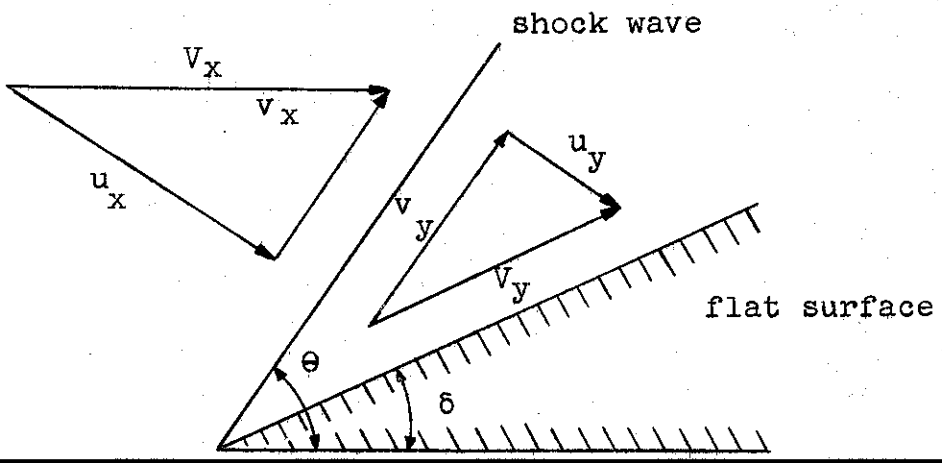

The fundamental relations derived in Reference 11, and/or obtained from Fig. E are:

A. Conservation of Momentum

$$\frac{P_y}{P_x} = 1 + \gamma_x M_x^2 \sin^2\theta \left[1 - \frac{u_y}{u_x}\right] \tag{6}$$

B. Conservation of Energy

$$\frac{h_y}{h_x} = 1 + \frac{\gamma_x - 1}{2} M_x^2 \sin^2\theta \left[1 - \left(\frac{u_y}{u_x}\right)^2\right] \tag{7}$$

C. Continuity

$$\rho_x u_x = \rho_y u_y \tag{8}$$

D. Equation of State, including real gas effects

$$P_y = \frac{R}{M_o} \cdot \rho_y T_y Z_y \tag{9}$$

E. Oblique Shock Wave Geometry (Fig. E)

$$\frac{u_y}{u_x} = \frac{\tan(\theta - \delta)}{\tan\theta} \tag{10}$$

$$\frac{M_y}{M_x} = \frac{u_y}{u_x} \cdot \frac{a_y}{a_x} \cdot \frac{\sin(\theta - \delta)}{\sin\theta} \tag{11}$$

Assuming all conditions in front of the shock known and all conditions aft of the shock unknown, the seven unknown parameters (p, h, ρ, u, T, Z, and θ) may be obtained by solving simultaneously the five equations (6), (7), (8), (9), and (10) along with the following two equations:

$$Z = Z(h,p) \tag{12}$$

and

$$T = T(h,p) \tag{13}$$

which are in the form of air tables. This set is solved numerically by iteration on a digital computer.

5. BOUNDARY CONDITIONS

Figure 5 illustrates the aerodynamic representation of the wedges including the shocks. With the method described in Sect. 4, the conditions existing after the first shocks (i.e. regions 1 and 2) can be obtained.

Shock interaction can be treated as shock reflection to obtain the conditions in regions 3 and 4. This involves setting the two following conditions:

1) the flow directions in regions 3 and 4 are the same

2) the static pressures in regions 3 and 4 are equal.

The existence of these conditions originate from the Continuity and Momentum equations. By considering the slipstream as a streamline, it can easily be seen that the flow direction and pressure must be the same on either side of it, i.e. in regions 3 and 4.

Condition 1 is used to define the equivalent deflection angles for regions 3 and 4 in terms of the unknown contact surface deflection angle, ϵ . These deflection angles are simply the angle between the flow directions before and after the second shocks. Thus the following equations can be obtained from Fig. 5 :

$$\delta_3 = \delta_1 + \epsilon \tag{14}$$

$$\delta_4 = \delta_2 - \epsilon \tag{15}$$

6. METHOD OF CALCULATION

The method used to calculate the parameters in all regions of the inlet is listed in this section. As can be seen from Section 4, to calculate the parameters across the first shocks, a method of iteration is used, since for a real gas the variation of Z and T can not be explicitly expressed in a form suitable for a direct solution of the equations (6), (7), (8), (9), (10), (12), and (13). Across the reflected shocks, a double iteration procedure is used. A given value for ϵ (contact surface angle) is assumed and the same method (i.e. oblique shock calculations) is used to calculate the parameters in the regions 3 and 4. Then a check is used to determine whether the pressures in regions 3 and 4 are the same (to within a given criterion). If it is, then the solution is complete, but if it is not then the False Point Method of iteration (Ref. 12) is used to determine a new value for ϵ, and the same procedure is repeated until the solution is acceptable. The solution is acceptable when the pressures on both sides of the contact surface are the same to within 5 significant figures.

6.1 Independent Parameters

1. Choose values for M_∞, α and d.

   The values chosen were:

M_∞	8 to 30 in steps of 2.
α	0° to 10° in steps of 2°.
d	5° to 30° in steps of 5°.

2. From Fig. 4 obtain a value of H (Altitude) corresponding to M_∞ for the Boost curve.

6.2 Calculation of Free Stream Properties

1. From the Atmospheric Equations (Ref. 9) listed in Appendix C calculate P_∞ and T_∞.
2. Assume $\gamma = 1.4$ and $Z = 1$.
3. Calculate h_∞, ρ_∞, a_∞, S_∞, and V_∞ from the following equations:

$$h_\infty = 0.12395\left(\frac{\gamma_\infty}{\gamma_\infty - 1}\right)\cdot T_\infty + 108.95 \tag{16}$$

$$\rho_\infty = \frac{p_\infty}{96.0298 T_\infty} \tag{17}$$

$$a_\infty = \sqrt{3089.7\gamma_\infty T_\infty} \tag{18}$$

$$S_\infty = 2.9128 + .9985 \operatorname{Log}\left(\frac{T_\infty}{273.16}\right) - .2854 \operatorname{Log}\left(\frac{P_\infty}{2116.2}\right) \tag{19}$$

$$V_\infty = a_\infty M_\infty \tag{20}$$

6.3 Calculation of Flow Parameters in Regions 1 and 2

1. Assume $\theta = 1.2\ \delta$.
2. Calculate u_y/u_x from equation (8).
3. Compute p_y and h_y from equations (6) and (7).
4. Enter air property tables at p_y and h_y to find T_y, Z_y, S_y, and a_y.
5. Compute γ_y from:

$$a_y = \sqrt{3089.7\gamma_y T_y Z_y} \tag{21}$$

6. Compute ρ_y from equation (9)
7. Combine equations (8) and (10) to get:

$$\frac{\rho_y}{\rho_x} = \frac{\tan\theta}{\tan(\theta - \delta)} \tag{22}$$

8. Compute a new value of θ (renamed θ_A) from equation (22) using the old value of tan θ.

9. Repeat steps 2 to 8 of above until the absolute value of $(\theta/\theta_A - 1)$ is less than 0.0001.

10. Calculate M_y from equation (11) (Sect. 4).

11. Print out all the useful parameters, such as p_y, T_y, M_y, h_y, ρ_y, Z_y, γ_y, S_y, a_y, and θ.

The above steps were done twice for deflection angles of δ_1 and δ_2 so as to obtain the conditions at regions 1 and 2.

6.4 Calculation of ϵ and the Flow Parameters in Region 3 and 4

1. Assume $\epsilon' = 2\alpha$

   This follows from equation (3) and the fact that the contact surface deflection angle (ϵ) may be taken as a rough approximation to be equal to the difference between the aerodynamic wedge angles δ_1 and δ_2 (Ref. 3).

2. Assume $\theta_3 = 1.2\ \delta_3$

   This is known to be a reasonable first approximation (Ref. 10,13).

3. Repeat steps 2 - 10 of the Oblique Shock Calculations (Sect. 6.3).

4. Assume $\theta_4 = 1.2\ \delta_4$

5. Repeat steps 2 - 10 of section 6.3

6. Assume $\epsilon'' = 2.0002$

   This value of ϵ'' is taken so that ϵ' and ϵ'' will not be too different in value.

7. Repeat steps 3 - 5 of above with e" instead of ϵ' .

8. Let $f' = \left| p'_3/p'_4 - 1 \right|$

This is the function which is to be minimized by the False Point Iteration.

9. Let $f'' = \left| p''_3/p''_4 - 1 \right|$

10. Calculate ϵ''' from the False Point Iteration Formula

$$\epsilon''' = \epsilon'' - f'' \cdot \frac{\epsilon' - \epsilon''}{f' - f''} \qquad (23)$$

11. Repeat steps 3 - 5 of above with ϵ''' instead of ϵ'.

12. Let $f''' = \left| p'''_3/p'''_4 - 1 \right|$

13. Test

Is $f''' \leq .0001$?

If YES go to 14b (solution is acceptable)

If NO go to 14a (solution is not acceptable; iterate again)

14a. Replace ϵ' by ϵ''

ϵ'' by ϵ'''

f' by f''

f'' by f'''

Repeat steps 10 - 13 of above.

14b. Print out ϵ and all required parameters in regions 3 and 4.

6.5 Air Tables

In the computer program four air tables are used. These are:

$Z = Z(h, \log p)$

$T = T(h, \log p)$

$S = S(h, \log p)$

$a = a(h, \log p)$

These tables are given in Appendix B . The method of inter-

polation between the values in the tables is linear and is described in Appendix B .

Only the first two tables are used in the actual solution, the others are merely to give additional information.

7. DISCUSSION OF RESULTS

The calculations described in this report were performed for the following Mach number - altitude combinations:

Mach	8	- 60,000 ft.	Mach	20	- 145,000 ft.
	10	- 78,000		22	- 156,000
	12	- 94,000		24	- 168,000
	14	- 108,000		26	- 178,000
	16	- 121,000		28	- 188,000
	18	- 135,000		30	- 198,000

At each of these conditions the wedge angles (d) were varied from 5° - 30° in steps of 5°, and the angle of attack (α) was varied from 0° to 6° in steps of 2°. This gives 300 distinct cases where $\alpha \leq d$.

A typical computer output sheet is enclosed in Appendix A . The first line under the heading gives the input parameters M5 (free stream Mach number), ALT(altitude), ALF(angle of attack), GEOMD(geometric wedge angle); and the aerodynamic wedge angles (D1 and D2), which are calculated from equations (1) and (2). The next five lines of data under various headings of thermodynamic and shock wave properties and their units refer to the regions ∞ (free stream), 1, 2, 3, and 4 in that order (Fig. 3). The second column of the next section gives the Mach number for the regions 1, 2, 3, and 4 in that order. The first column specifies the ratio (or difference in the case of entropy) of the various properties in the different regions of figure 3 . For example T/T opposite 2/5 means T_2/T_∞, while DEL S opposite 4/5 means $S_4 - S_\infty$ (in BTU/lb - °K). The next line gives the co-ordinates of the

interaction point (XC , YC) and the two places where the interacted (second) shocks hit the wedges (XD, YD and XE, YE). These co-ordinates (Fig. 23- 25) are calculated by assuming the tip of the bottom wedge as the origin, and an intake height of unity. The angular deflection of the contact surface from the free stream flow direction (EPS) is printed on the last line of the computer output sheet.

There exist two possibilities that the computer program will not give complete answers for a given case.

The first one occurs when the oblique shock calculations require more than the maximum specified number of iterations (15 iterations) allowed for the program to converge to the required criterion (See Sect. 6). This would cause the particular calculation to cease and the computer would print:

"OBSHOK ITERATION DOES NOT CONVERGE"

(see sample sheet in Appendix A). The computer would then proceed to the next case. The second possibility occurs when the value of pressure or enthalpy is out of range of the Mollier air tables that were fed into the computer. This would cause the calculation to cease and the computer to print:

"OUT OF RANGE OF AIR TABLES"

(see sample sheet in Appendix A). The computer would then proceed to the next case.

The accuracy of the final results depends on a number

erties vary with the season, the latitude, and the time of day. Thus, a Standard Atmosphere (Ref. 9) was used in the calculations. The Mollier Charts are given to 5 significant figures and it is not known how many of these are truly exact especially at high enthalpies.

Boundary layer effects were not included in the calculation. This is not really a source of error if it is considered that the deflection angles (δ) are the deflections of the fluid and not the physical deflection of the wedge surfaces.

The size of the criterion is a source of error since a criterion always has to be specified. The criterion used was such as to give pressures, across the contact surface, significant to five figures. Since pressure is very sensitive to a change in flow deflection angle, good accuracy is achieved. Ten significant figures were used in all computer calculations. Using only five figures would result in the fifth significant figure being doubtful.

It should be noted that all the oblique shock and thermodynamic equations used are exact and thus do not contribute to any errors.

Figure 4 shows the Flight Corridor. All the calculations described in this report are for the Boost path. Along this path the equilibrium skin temperature of the surface ranges from 1100°K to 1850°K (Ref. 14) as the free stream Mach number varies from 8 to 30. The earth satellite speed (shown on Fig. 4 as a zigzag line) is the speed that a winged hypersonic vehicle would have to reach for the centrifugal

force to equal the force of gravity.

Figures 6 and 7 are Altitude - Temperature and Altitude - Pressure Charts for a Standard Atmosphere. These were used in our calculations. These are included as they can be combined with Fig. 4 to show the variation of temperature and pressure along the Boost path.

All the results on figures 8 to 16 are plotted against the free stream Mach number (M_∞), with the aerodynamic wedge angles (δ) as parameters. These graphs represent wedges with equal aerodynamic angles (δ) since there is no angle of attack of the free stream flow.

Figure 8 shows M_1, the Mach number after the first shock versus M_∞ . For a constant δ, M_1 increases with M_∞ while at a constant M_∞ , M_1 decreases with an increase in δ. It should be noted that for $\delta = 10°$, M_1 varies from 6 to 11.3 as M_∞ goes from 8 to 30.

Reference 14 shows that optimum hypersonic ramjet performance is obtained with an intake which reduces the free stream Mach number by a factor of 3. On Fig. 9 (M_3 vs. M_∞), this optimum line is shown dashed and this line is seen to lie in the vicinity of $\delta = 10°$ to 15°, being closer to 10° in high Mach number region and closer to 15° in the low Mach number region.

For the range of interest to hypersonic ramjets (i.e. $15° > \delta > 10°$), the pressure ratio, p_3 / p_∞ (Fig. 10), varies from 40 to 330 and the temperature ratio, T_3 / T_∞ (Fig. 12), varies from 3.7 to 10.7 as the free stream Mach number

varies from 8 to 30. The shape of the curves in Fig. 12 is caused by the shape of the Altitude-Temperature relation (Fig. 6) and by the kinks in the air tables. These kinks are caused by a variation in the specific heats.

Figures 11 and 13 show the actual pressure ($p_3 = p_4$) and temperature ($T_3 = T_4$) versus the free stream Mach number for various geometric wedge angles. For the range of interest to hypersonic ramjets, the pressure varies from 1.1 to 40 psi, and the temperature from 820 to 2720° K.

Although the density ratios were calculated, they were not plotted. It should be noted that across the contact surface the density ratio (ρ_3 / ρ_4) is inversely proportional to the temperature ratio (T_3 / T_4). This is accurate because

$$p_3 = p_4 \quad \text{and} \quad Z_3 \doteq Z_4$$

Fig. 14 shows the intake height ratio (or effectively the area ratio) versus M_∞. For the hypersonic ramjet range of interest, the area ratio varies from 0.11 to 0.035 as M_∞ varies from 8 to 30.

Fig. 15 shows the relative position of the point of interaction versus M_∞. Figure 16 shows the ratio of intake length to height versus M_∞. It can be seen that for high free stream Mach numbers the above distance ratios remain reasonably constant.

Figure 17 is a graph of the Contact Surface Deflection Angle versus M_∞ for various Wedge Deflection Angles. It should be noted that the curves tend to bunch in groups according to the difference of the wedge angles ($\delta_2 - \delta_1$).

Molder (Ref. 3) has shown that for an ideal gas, the contact surface deflection angle (ϵ) is approximately equal to the difference of the aerodynamic wedge angles. From these graphs, it can be observed that ϵ is always less than $(\delta_2 - \delta_1)$, but tends toward it at low Mach numbers. Another important feature of these two graphs is that a minimum point can be seen on a few curves.

Figures 18 to 25 are all plotted versus the angle of attack (α) with the free stream Mach number (M_∞) as parameter. These graphs were plotted for equal geometric wedge angles (d) of 10°.

Figure 18 is a graph of the Contact Surface Deflection Angle (ϵ) and the Actual Geometrical Contact Surface Deflection Anlge ($\epsilon - \alpha$), i.e. the angle by which the flow is deflected from the centerline of the wedge intake, versus α and M_∞. A line of $\epsilon = \alpha$ is also plotted. The significant feature of this graph is that ϵ is always grater than α.

Figure 19 is a graph of the Mach number in region 3 and 4 versus α and M_∞. It should be noted that for any given M_∞, the difference between M_3 and M_4 is small.

Figure 20 is a graph of the pressure in region 3 or 4 versus α and M_∞. It should be noted that for a given M_∞, the change in pressure is small for a change in α.

Figure 21 is a graph of the temperature in regions 3 and 4 versus α and M_∞. It should be noted that the temperature difference across the contact surface increases with an increase in the angle of attack (α).

Figures 22 to 25 are graphs of the geometry of the wedge intakes versus α and M_∞. Figure 22 shows the ratio of the distance of the points D and E (See diagram on Fig. 22-25) from the intake entrance to the intake height. It should be noted that practically all the lines are linear and that point E is further back than point D. It is also important that point D moves back while point E moves forward with an increase in the angle of attack. Figure 23 shows the ratio of the heights of points D and E to the intake height. This graph confirms the relative position of D and E as discussed for Fig. 22. Figures 24 and 25 are the graphs of the ratio of the X and Y co-ordinates of the point of interaction to the intake height. It is observed that the distance of the interaction point from the intake entrance increases with an increase in M_∞, while it decreases very slightly for an increase in α. It can be seen (Fig. 25) that the effect of M_∞ on the height of the point of interaction is small.

Figures 26 to 29 describe the performance of the hypersonic intake (Ref. 8). This performance is described in terms of two parameters: (1) the "Efficiency" and (2) the "Capability".

$$C_{KE_x} = 1 - \left[\frac{V_x}{V_\infty}\right]^2$$

This coefficient increases with an increase in capability between the limits of 0 and 1.

Figure 27 shows the effect of a variation of α on the non-dimensional entropy change. On the compression side $(\Delta S / R)_4$ increases almost linearly with α, whereas on the expansion side, the decrease is non-linear. The increase in $\Delta S / R$ is larger than the decrease; consequently, the intake becomes less efficient with an increase in α.

Figure 29 shows the effect of a variation of α on C_{KE}. On the compression side, C_{KE_4} increases almost linearly with α , whereas on the expansion side, the decrease is non-linear. The increase in C_{KE} is larger than the decrease; consequently, the intake increases capability with an increase in the angle of attack.

8. CONCLUSIONS

This report presents the calculated thermodynamic and oblique shock data for hypersonic double oblique shock waves. This was done for a real gas (air) along a Mach number - altitude relationship representative of possible hypersonic ramjet flight capabilities. Results are given for the dynamic and thermodynamic variables during and after the shock interaction, and also for the geometry of the interaction. Results are calculated for various wedge angles and Mach numbers. A detailed examination of the effect of angles of attack is included. Throughout, special emphasis is placed on conditions which are thought to be suitable for the use of the double oblique shock system as an intake for hypersonic ramjets.

For optimum intake performance over a Mach number range from 8 to 26, it is required that the flow deflection (wedge angles) be changed from 15 deg. to 10 deg. The compression ratio (p_3 / p_∞) of such a variable intake ranges from 40 to 240. The actual maximum pressure in the intake occurs at the lowest Mach number and reaches a value of 40 psia. The maximum static temperature in the intake (at Mach 26) is 2600° K. The contraction ratio (area ratio) varies from 0.11 to 0.041. At hypersonic speeds, the position of the shock interaction point (C) and the reflected shock impingement points (D and E) are seen to be insensitive to a variation in Mach number. If boundary layer suction is applied at the reflected shock impingement points to alleviate shock boundary layer interaction effects, then the fact that the shocks do not move appreciably

means that suction does not have to be applied over a large area.

As with ideal gases (Ref. 3), the contact surface deflection angle (ϵ) is almost equal to the difference between the aerodynamic wedge angles ($\delta_2 - \delta_1$). The deflection angle is always slightly lower than the difference in the aerodynamic wedge angles, this difference increasing with an increase in aerodynamic wedge deflection angles. For every pair of unequal aerodynamic wedge deflection angles, there exists a Mach number at which ϵ is a minimum.

For angles of attack up to 6 deg., the variation of with angle of attack (α) is linear and relatively insensitive to the free stream Mach number. The net flow deflection ($\epsilon - \alpha$) is always opposite to the angle of attack and slightly less than the angle of attack, so that the pair of wedges act as a flow turning mechanism. ($\epsilon - \alpha$) is the angle through which the flow must be turned back to resume the axial direction in the combustion chamber. It is seen that ($\epsilon - \alpha$) decreases with an increase in the free stream Mach number.

A comparison of M_3 and M_4 versus α shows for the whole Mach number range that there is not a great deal of non-uniformity due to variations in the angle of attack. The difference of Mach numbers (M_3 and M_4) is typically of the order of 8%. An increase in angle of attack leads to a slight decrease in pressure ($p_3 = p_4$), and compression ratio.

For a 10 deg. deflection angle, the static temperatures at the exit of the intake (after shock interaction) are high

enough to lead to spontaneous ignition of most fuels.

The reflected shock which impinges on the surface at the higher angle to the stream impinges at a point (E) which is further from the entrance plane than the corresponding shock impingement point on the opposite surface. At lower Mach numbers (8 and 10), the distance (X_E) of point E from the entrance plane (Fig. 22) does not seem to be affected by a variation in the angle of attack.

From figures 24 and 25, it is seen that (except for Mach 30) the point of interaction moves forward and up with an increase in the angle of attack.

For hypersonic air intakes (Ref. 8), two parameters of importance are the efficiency as expressed by the entropy increase ($\Delta S/R$), and the capability, as expressed by the kinetic energy coefficient (C_{KE}). Figure 26 shows the non-dimensional entropy increase as varying from 0.5 to 4.2. This is in substantial agreement with the corresponding values given by ideal gas calculations (Ref. 8). Ramjet performance calculations are in progress to see whether this type of intake gives high enough performance to be practically suitable. The non-dimensional entropy increase through the lower shock system is higher by 0.5 (on the average) than that through the higher shock system. Values of C_{KE} are highest at the high deflection angles and decrease slightly with an increase in the free stream Mach number. The shock system which more nearly faces the free stream direction, i.e. the lower pair of shocks,

gives rise to higher values of C_{KE} than the upper pair of shocks.

In general , this type of intake is found to be relatively insensitive to variations in Mach number and angle of attack.

9. REFERENCES

1. Mach, E.
Vienna Acadamy. Sitzeingeberichte 77, 891
(1878)

2. Ames Research Staff
Equations, Tables and Charts for Compressible Flow
NACA Report 1135 (1953)

3. Molder, S.
Head-on Interaction of Oblique Shock Waves
Institute of Aerophysics, University of Toronto,
Tech. Note No. 38 (Sept 1960)

4. Smith, L.G.
Photographic Investigation of the Reflection of Plane Shocks in Air.
OSRD Rep. 6271 (1951)

5. Keenan, P.C. and Seeger, R.J.
Analysis of Data on Shock Intersections.
Progress Report I, U.S. Navy, Bur. Ord.,
Explosives Research Report 15 (1944)

6. Polachek, H. and Seeger, R.J.
Analysis of Data on Shock Intersections
Progress Report II, U.S. Navy, Bur. Ord.
Report 417

7. Shapiro, A.H.
The Dynamics and Thermodynamics of Compressible Fluid Flow,
Volumes I and II,
Ronald Press Co., New York, (1953)

8. Molder, S.
Intakes for Hypersonic Ramjets
Mechanical Engineering Research Laboratories,
McGill University
Report 62-6, (July 1962)

9. Evered, R.D.
Atmospheric Data,
The A.R.D.C. Model Atmosphere 1956
Ramjet Dept., Bristol Siddeley Engines Ltd.,
Report No. 2560, (June 1959)

10. Normal and Oblique Shock Characteristics at Hypersonic Speeds.
Douglas Aircraft Co., Inc.,
Engineering Report No. LB-25599, (Dec. 1957)

11. Moeckel, W.E.
Oblique Shock Relations at Hypersonic Speed for Air in Chemical Equilibrium,
NACA Technical Note 3895, (Jan. 1957)

12. Stanton, R.G.
Numerical Methods for Science and Engineering
Prentice Hall Inc., New Jersey, (1961)

13. Normal and Oblique Shock Characteristics at Hypersonic Speeds.
Douglas Aircraft Co., Inc.,
Engineering Report No. LB-25599, Supp. I, (Feb. 1959)

14. Molder, S.
Cruise and Boost Performance of Hypersonic Ramjets
Mechanical Engineering Research Laboratories,
McGill University,
Tech. Note. 62-3, (July, 1962).

APPENDIX B

AIR TABLE INTERPOLATION

The interpolation formula illustrated and listed below is one of linear interpolation.

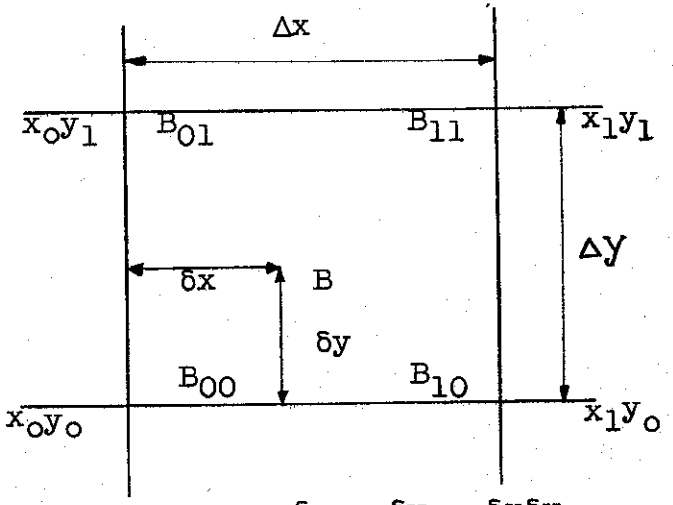

$$B = B_{00}\left(1 - \frac{\delta x}{\Delta x} - \frac{\delta y}{\Delta y} + \frac{\delta x \delta y}{\Delta x \Delta y}\right)$$

$$+ B_{10}\left(\frac{\delta x}{\Delta x} - \frac{\delta x \delta y}{\Delta x \Delta y}\right)$$

$$+ B_{01}\left(\frac{\delta y}{\Delta y} - \frac{\delta x \delta y}{\Delta x \Delta y}\right)$$

$$+ B_{11}\left(\frac{\delta x \delta y}{\Delta x \Delta y}\right)$$

For the four Mollier Air Tables the format and the co-ordinates are identical. The abscissa represents the enthalpy and the ordinate the log of the pressure. These four tables are illustrated on the following pages.

h \ $Log_{10}P$ (P)	.0001 (-4.0)	-3.5	.001 (-3.0)	-2.5	.01 (-2.0)	-1.5	.1 (-1.0)	-0.5	1.0 (0.0)	+0.5	10 (+1.0)	+1.5	100 (+2.0)
0	1.0000	1.0000	1.0000	1.0000	1.0000	1.0000	1.0000	1.0000	1.0000	1.0000	1.0000	1.0000	1.0000
200	1.0000	1.0000	1.0000	1.0000	1.0000	1.0000	1.0000	1.0000	1.0000	1.0000	1.0000	1.0000	1.0000
400	1.0000	1.0000	1.0000	1.0000	1.0000	1.0000	1.0000	1.0000	1.0000	1.0000	1.0000	1.0000	1.0000
600	1.0000	1.0000	1.0000	1.0000	1.0000	1.0000	1.0000	1.0000	1.0000	1.0000	1.0000	1.0000	1.0000
800	1.0001	1.0001	1.0000	1.0000	1.0000	1.0000	1.0000	1.0000	1.0000	1.0000	1.0000	1.0000	1.0000
1000	1.0028	1.0035	1.0041	1.0023	1.0004	1.0003	1.0001	1.0001	1.0000	1.0000	1.0000	1.0000	1.0000
1200	1.0179	1.0133	1.0087	1.0065	1.0042	1.0030	1.0017	1.0010	1.0003	1.0003	1.0002	1.0002	1.0001
1400	1.0327	1.0280	1.0233	1.0189	1.0145	1.0110	1.0075	1.0049	1.0023	1.0017	1.0011	1.0008	1.0004
1600	1.0528	1.0472	1.0415	1.0355	1.0295	1.0240	1.0184	1.0139	1.0094	1.0067	1.0039	1.0027	1.0014
1800	1.0741	1.0677	1.0613	1.0543	1.0473	1.0374	1.0274	1.0235	1.0196	1.0142	1.0087	1.0063	1.0038
2000	1.0960	1.0891	1.0822	1.0744	1.0665	1.0581	1.0496	1.0411	1.0325	1.0252	1.0179	1.0129	1.0079
2200	1.1182	1.1108	1.1034	1.0950	1.0866	1.0771	1.0676	1.0576	1.0476	1.0381	1.0286	1.0200	1.0114
2400	1.1402	1.1325	1.1248	1.1159	1.1069	1.0967	1.0865	1.0752	1.0639	1.0526	1.0412	1.0316	1.0219
2600	1.1622	1.1544	1.1465	1.1369	1.1273	1.1165	1.1057	1.0934	1.0810	1.0681	1.0551	1.0433	1.0315
2800	1.1827	1.1769	1.1710	1.1619	1.1527	1.1388	1.1248	1.1119	1.0989	1.0844	1.0698	1.0560	1.0422
3000	1.1984	1.1917	1.1850	1.1757	1.1664	1.1550	1.1436	1.1298	1.1160	1.1006	1.0852	1.0695	1.0538

$Z = Z(h, \text{Log}P)$

h -- Btu/lb.

P -- Atm.

$$Z = \frac{\mu_o}{\mu} = \frac{28.85}{\mu}$$

MOLLIER AIR TABLE I

h \ Log_{10} P	P → .0001 -4.0	.0003162 -3.5	.001 -3.0	.003162 -2.5	.01 -2.0	.03162 -1.5	.1 -1.0	.3162 -0.5	1.0 0.0	3.162 +0.5	10 +1.0	31.62 +1.5	100 +2.0
0	-252.9	-252.9	-252.9	-252.9	-252.9	-252.9	-252.9	-252.9	-252.9	-252.9	-252.9	-252.9	-252.9
200	211.3	211.3	211.3	211.3	211.3	211.3	211.3	211.3	211.3	211.3	211.3	211.3	211.3
400	665.0	665.0	665.0	665.0	665.0	665.0	665.0	665.0	665.0	665.0	665.0	665.0	665.0
600	1082.4	1082.4	1082.4	1082.4	1082.4	1082.4	1082.4	1082.4	1082.4	1082.4	1082.4	1082.4	1082.4
800	1471.1	1471.4	1471.8	1471.9	1472.1	1472.1	1472.1	1472.1	1472.1	1472.1	1472.1	1472.1	1472.1
1000	1802.7	1814.2	1825.6	1830.9	1836.2	1838.1	1840.0	1840.5	1841.0	1841.3	1841.6	1841.8	1841.9
1200	2000.4	2040.2	2080.0	2109.4	2138.8	2155.7	2172.6	2179.8	2187.0	2189.5	2191.9	2192.8	2193.7
1400	2113.5	2174.0	2234.5	2287.7	2348.0	2392.9	2437.7	2465.6	2493.4	2505.8	2518.2	2522.9	2527.6
1600	2196.8	2269.5	2342.1	2418.7	2495.2	2564.5	2633.7	2688.9	2744.2	2778.2	2812.1	2827.3	2842.4
1800	2261.1	2344.3	2427.4	2516.6	2605.8	2694.9	2783.9	2864.8	2945.6	3006.2	3066.7	3100.8	3134.9
2000	2321.9	2411.7	2501.5	2599.9	2698.3	2802.5	2906.7	3009.2	3111.6	3198.9	3286.1	3344.6	3403.0
2200	2378.5	2473.4	2568.2	2666.2	2764.2	2888.6	3013.0	3132.9	3252.8	3364.6	3476.4	3561.4	3646.4
2400	2439.4	2537.9	2636.3	2748.3	2860.2	2985.9	3111.6	3246.0	3380.4	3513.3	3646.2	3751.6	3856.9
2600	2504.1	2605.4	2706.7	2823.9	2941.2	3073.8	3206.3	3353.1	3499.8	3651.2	3802.6	3938.7	4074.7
2800	2592.3	2691.5	2790.7	2909.6	3028.5	3165.8	3303.0	3459.2	3615.4	3782.4	3949.4	4108.4	4267.4
3000	2734.5	2817.9	2901.2	3016.2	3131.1	3269.5	3407.9	3570.7	3733.4	3912.9	4092.5	4271.7	4450.8

Note: h = 108.95 Btu/lb. when T = 0°K

T -- °K

h -- Btu/lb.

P -- Atm.

$$T = T (h, \text{Log } P)$$

MOLLIER AIR TABLE II

h \ Log P (P →)	.0001 -4.0	-3.5	.001 -3.0	-2.5	.01 -2.0	-1.5	.1 -1.0	-.5	1.0 0	.5	10 1.0	1.5	100 2.0
0	3.4308	3.2886	3.1463	3.0041	2.8619	2.7198	2.5777	2.8710	2.2933	2.3022	2.0089	1.8489	1.6889
200	3.9359	3.7937	3.6515	3.5094	3.3672	3.2251	3.0829	2.9407	2.7985	2.6564	2.5142	2.3631	2.2120
400	4.4410	4.2989	4.1567	4.0146	3.8725	3.7303	3.5881	3.4459	3.3037	3.1616	3.0195	2.8773	2.7351
600	4.6744	4.5324	4.3904	4.2482	4.1060	3.9629	3.8218	3.6796	3.5374	3.3988	3.2602	3.1156	2.9709
800	4.8326	4.6907	4.5488	4.4069	4.2649	4.1239	3.9829	3.8393	3.6956	3.5532	3.4108	3.2685	3.1262
1000	4.9543	4.8119	4.6694	4.5271	4.3848	4.2426	4.1004	3.9582	3.8160	3.6708	3.5255	3.3865	3.2474
1200	5.0589	4.9152	4.7714	4.6283	4.4852	4.3427	4.2001	4.0579	3.9157	3.7735	3.6313	3.4891	3.3469
1400	5.1557	5.0096	4.8634	4.7187	4.5740	4.4304	4.2867	4.1440	4.0012	3.8588	3.7163	3.5740	3.4317
1600	5.2486	5.0996	4.9505	4.8036	4.6566	4.5110	4.3654	4.2213	4.0772	3.9343	3.7913	3.6487	3.5060
1800	5.3375	5.1859	5.0342	4.8846	4.7349	4.5871	4.4392	4.2933	4.1474	4.0032	3.8590	3.7160	3.5730
2000	5.4250	5.2705	5.1160	4.9632	4.8103	4.7139	4.6174	4.4154	4.2134	4.0677	3.9220	3.7782	3.6344
2200	5.5102	5.3523	5.1947	5.0388	4.8832	4.7301	4.5770	4.4267	4.2763	4.1288	3.9812	3.8376	3.6940
2400	5.5931	5.4321	5.2711	5.1126	4.9540	4.7982	4.6424	4.4902	4.3380	4.1902	4.0424	3.9033	3.7442
2600	5.6749	5.5107	5.3465	5.1847	5.0229	4.8643	4.7056	4.5503	4.3949	4.2430	4.0910	3.9427	3.7944
2800	5.7533	5.5863	5.4193	5.2547	5.0900	4.9286	4.7671	4.6093	4.4514	4.2970	4.1425	3.9925	3.8425
3000	5.8288	5.6593	5.4898	5.3225	5.1552	4.9910	4.8267	4.6660	4.5052	4.3663	4.2273	4.0579	3.8884

S -- Btu/lb-°K

h -- Btu/lb.

P -- Atm.

$S = S (h, \text{Log } P)$

MOLLIER AIR TABLE III

h \ Log P (P)	.0001 -4.0		.001 -3.0		.01 -2.0		0.1 -1.0		1.0 0.0		10 +1.0		100 +2.0
		-3.5		-2.5		-1.5		-0.5		+0.5		+1.5	
0	0	0	0	0	0	0	0	0	0	0	0	0	0
200	954.4	954.4	954.4	954.4	954.4	954.4	954.4	954.4	954.4	954.4	954.4	954.4	954.4
400	1675.9	1675.9	1675.9	1675.9	1675.9	1675.9	1675.9	1675.9	1675.9	1657.9	1675.9	1675.9	1675.9
600	2108.8	2108.7	2108.6	2108.6	2108.6	2108.6	2108.6	2108.6	2108.6	2108.6	2108.6	2108.6	2108.6
800	2432.5	2434.1	2435.6	2436.2	2436.7	2436.9	2437.0	2437.0	2437.0	2437.0	2437.1	2437.1	2437.1
1000	2609.8	2635.6	2661.3	2675.2	2689.0	2694.6	2700.1	2702.0	2703.9	2704.6	2705.2	2705.5	2705.8
1200	2680.1	2720.4	2760.6	2799.1	2837.6	2864.8	2891.9	2905.6	2919.3	2925.1	2930.8	2932.2	2933.5
1400	2747.8	2793.5	2839.1	2884.6	2930.0	2972.8	3015.5	3048.0	3080.5	3098.1	3115.6	3122.9	3130.1
1600	2817.8	2865.6	2913.3	2963.5	3013.6	3063.3	3113.0	3157.8	3202.6	3235.2	3267.7	3284.8	3301.8
1800	2884.0	2935.0	2986.0	3039.9	3093.7	3148.5	3203.2	3255.9	3308.5	3352.5	3396.5	3424.9	3453.3
2000	2951.2	3004.6	3057.9	3114.9	3171.9	3231.1	3290.2	3348.7	3407.1	3459.7	3512.2	3551.1	3590.0
2200	3020.3	3075.8	3131.3	3190.8	3250.3	3293.7	3376.1	3439.4	3502.7	3562.0	3621.3	3668.9	3716.4
2400	3098.2	3153.9	3209.5	3270.5	3331.5	3397.1	3462.6	3530.0	3597.3	3662.2	3727.0	3782.0	3836.9
2600	3183.2	3238.5	3293.8	3356.1	3418.3	3484.8	3551.3	3621.9	3692.5	3762.0	3831.5	3892.5	3953.5
2800	3305.0	3351.7	3398.4	3456.9	3515.3	3580.9	3646.4	3718.6	3790.7	3863.4	3936.1	4030.1	4124.0
3000	3513.0	3527.6	3542.1	3687.7	3633.3	3693.1	3752.8	3823.5	3894.1	3968.2	4042.3	4112.1	4181.8

a -- fps

h -- Btu/lb.

$a = a (h, \text{Log } P)$

P -- Atm.

MOLLIER AIR TABLE IV

APPENDIX C

ATMOSPHERIC EQUATIONS

Take geopotential altitude H in metres

Pressure in lbs/ft.^{2}

0 - 11,000m

$$P = \frac{2116.21695}{\left\{\frac{288.160}{288.160 - 6.5 \times 10^{-3} H}\right\}^{5.256,122,18}}$$

11,000 - 25,000 m

$$P = \frac{P_{11}}{\text{antilog}_{10}\left\{(.068,483,253 \times 10^{-3})(H - 11,000)\right\}}$$

25,000 - 47,000 m

$$P = \frac{P_{25}}{\left\{\frac{141.660 + 3. \times 10^{-3} H}{216.660}\right\}^{11.388,264.73}}$$

47,000 - 53,000 m

$$P = \frac{P_{47}}{\text{antilog}_{10}\left\{(.052,492,682,3 \times 10^{-3})(H - 47,000)\right\}}$$

53,000 - 75,000 m

$$P = \frac{P_{53}}{\left\{\frac{282.66}{489.36 - 3.9 \times 10^{-3} H}\right\}^{8.760,203,64}}$$

75,000 - 90,000 m

$$P = \frac{P_{75}}{\text{antilog}_{10}\left\{(.075,371,236,4 \times 10^{-3})(H - 75,000)\right\}}$$

Temperature in °K

0 - 11,000 m $\quad T = 288.16 - .0065\ H$

11,000 - 25,000 m $\quad T = 216.66$

25,000 - 47,000 m	$T = 216.66 + .003\ (H - 25{,}000)$
47,000 - 53,000 m	$T = 282.66$
53,000 - 75,000 m	$T = 282.66 - .0039\ (H - 53{,}000)$
75,000 - 90,000 m	$T = 196.86$

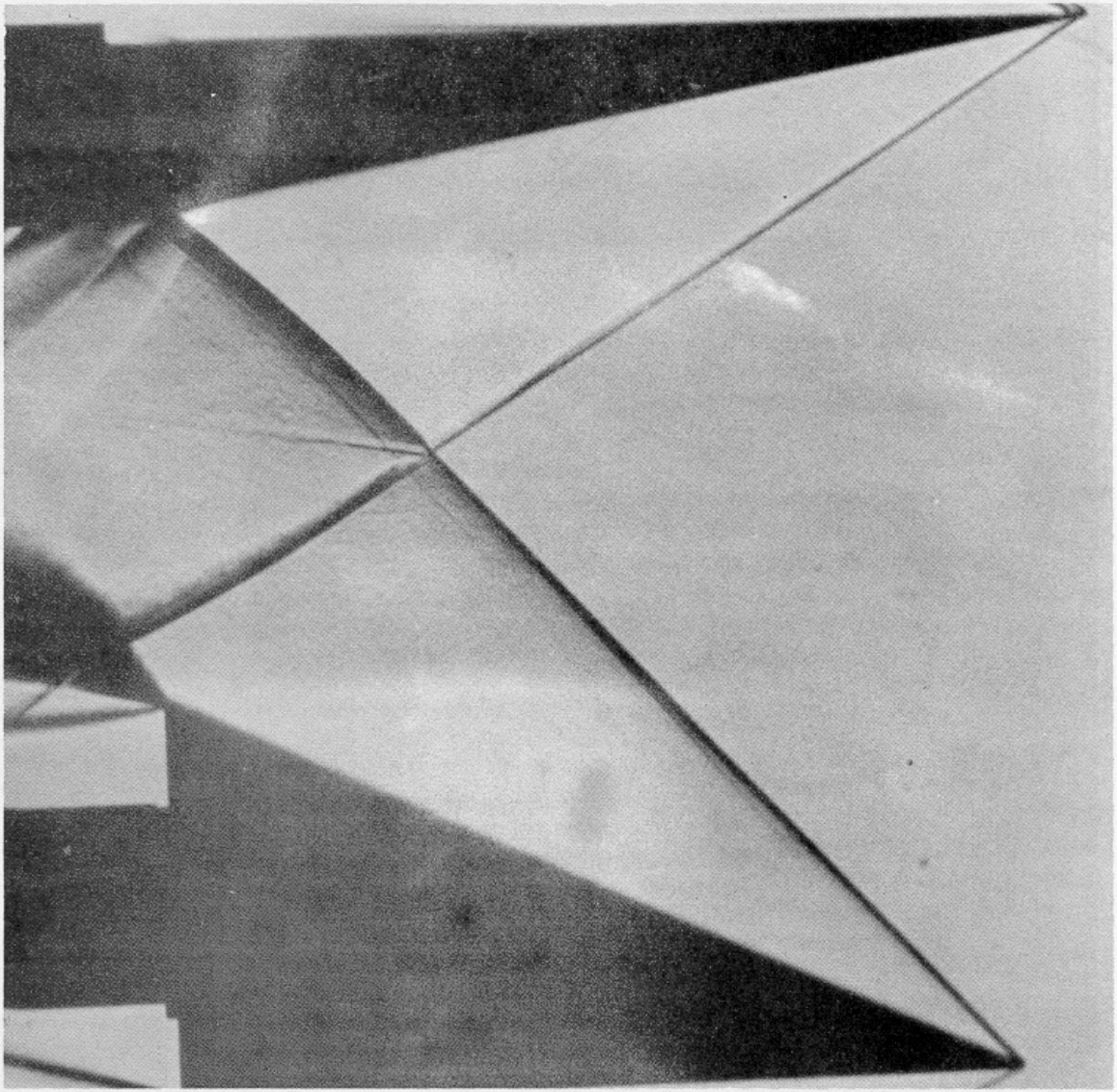

FIG. 1 SCHLIEREN PHOTOGRAPH OF REGULAR SHOCK INTERACTION. LOWER SURFACE OF UPPER WEDGE IS INCLINED 14 DEG. TO THE FLOW. UPPER SURFACE OF LOWER WEDGE IS INCLINED 21 DEG. TO THE FLOW. (Ref. 3)

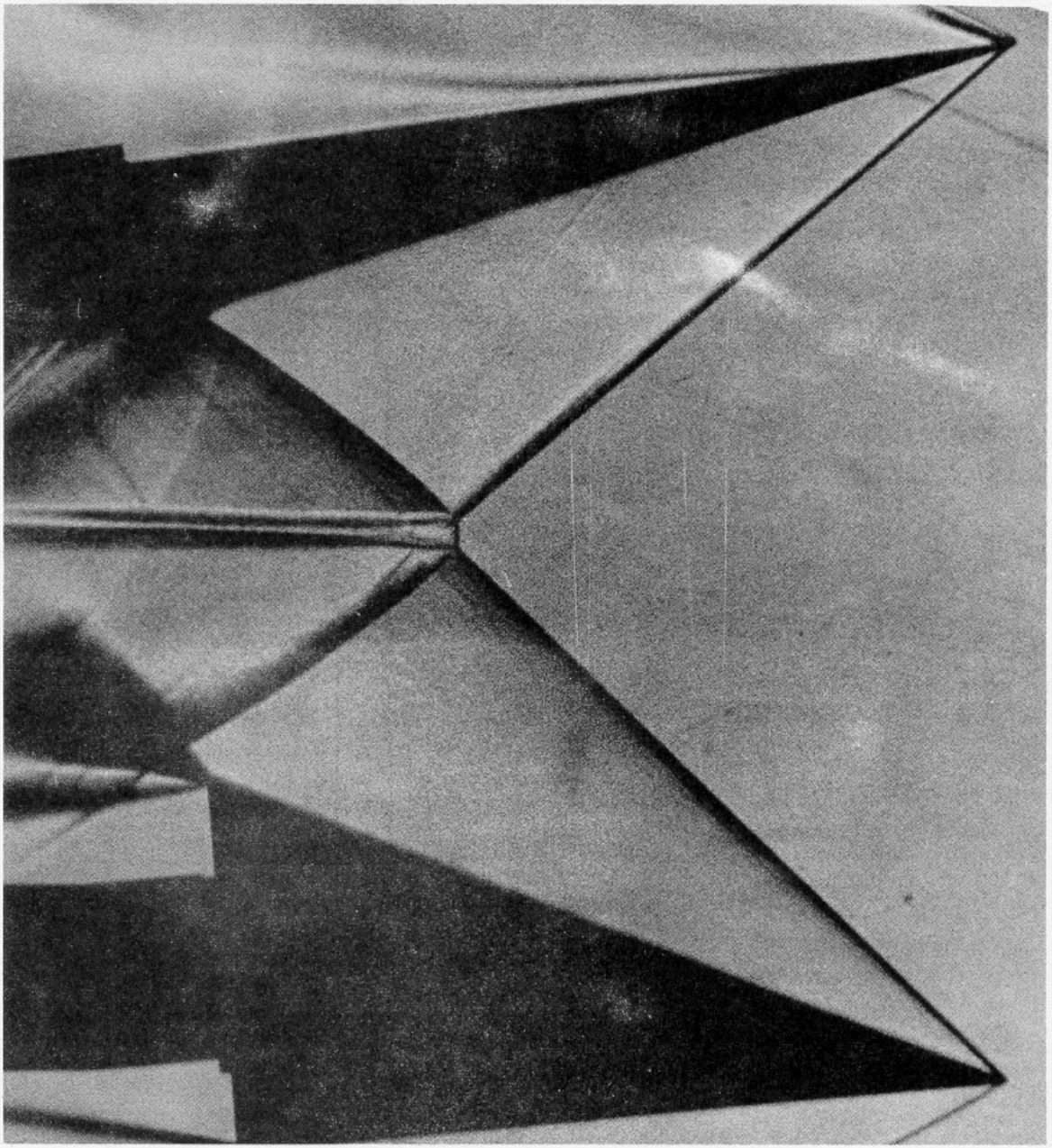

FIG. 2 SCHLIEREN PHOTOGRAPH OF MACH INTERACTION. LOWER SURFACE OF UPPER WEDGE IS INCLINED 15 DEG. TO THE FLOW. UPPER SURFACE OF LOWER WEDGE IS INCLINED 20 DEG. TO THE FLOW. (Ref. 3)

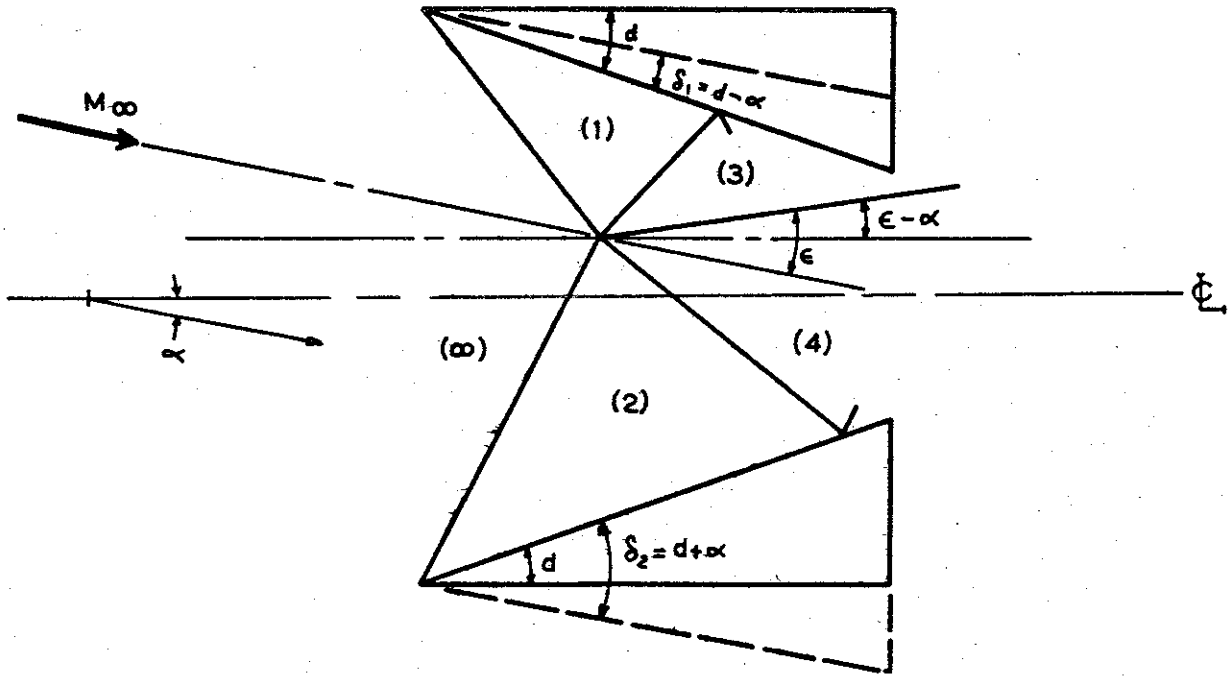

FIG. 3 DOUBLE WEDGE INTAKE WITH TWO INTERACTING OBLIQUE SHOCK WAVES

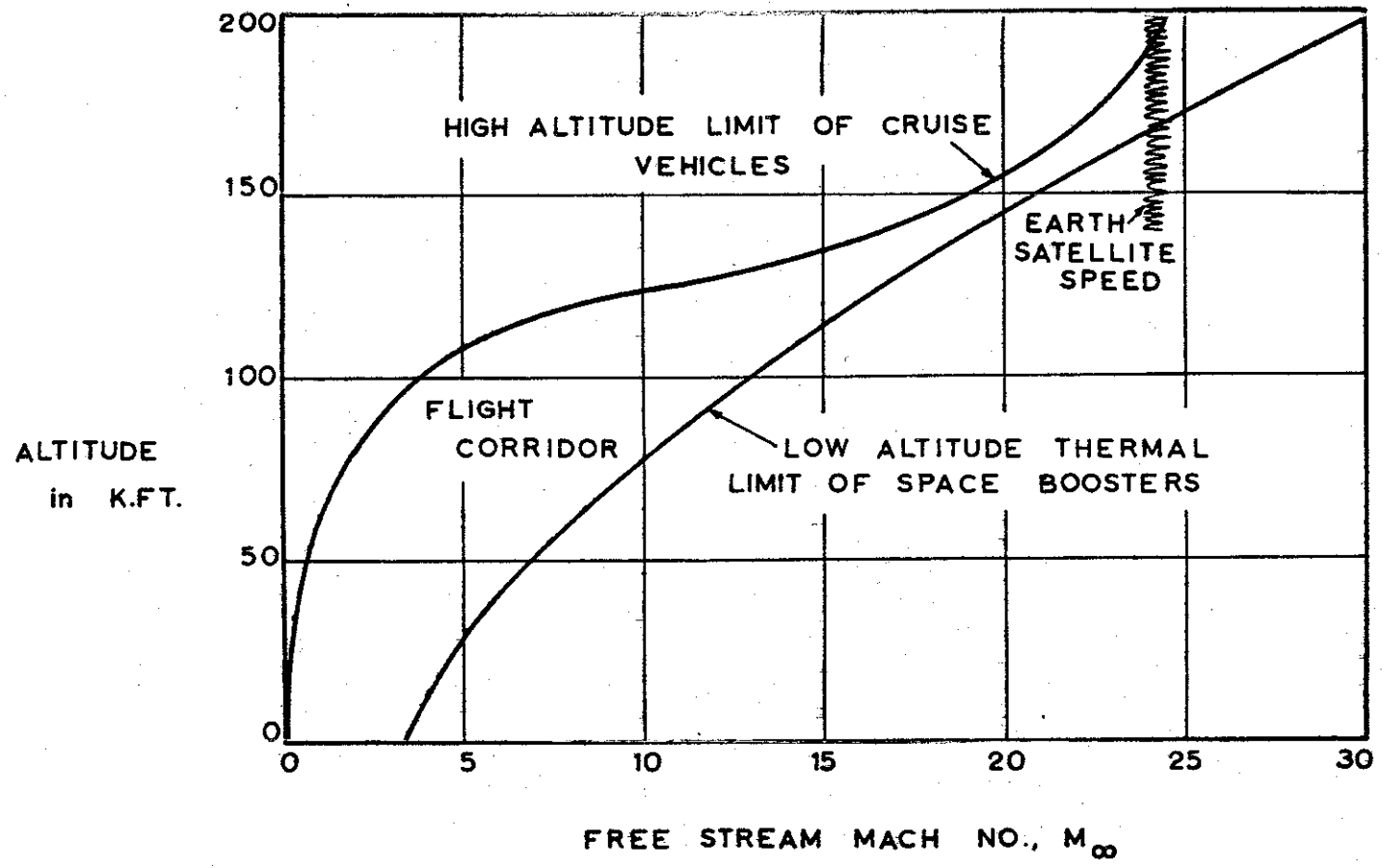

FIG. 4 THE FLIGHT CORRIDOR

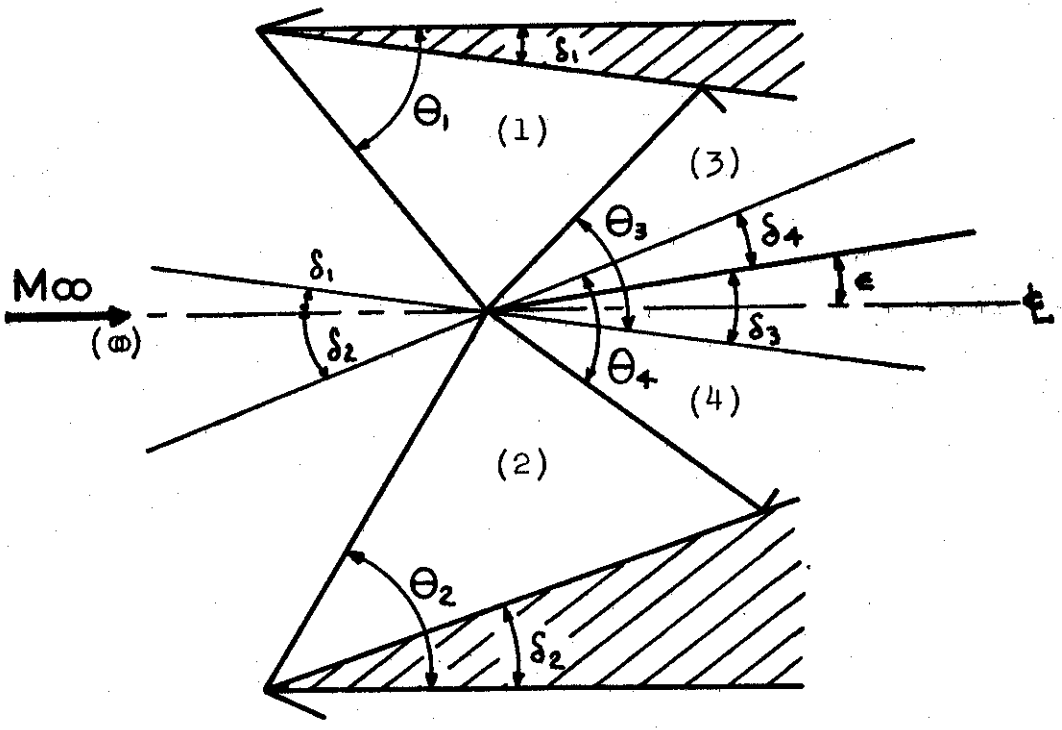

FIG. 5 AERODYNAMIC REPRESENTATION OF INLETS INCLUDING SHOCKS AND DEFLECTION ANGLES

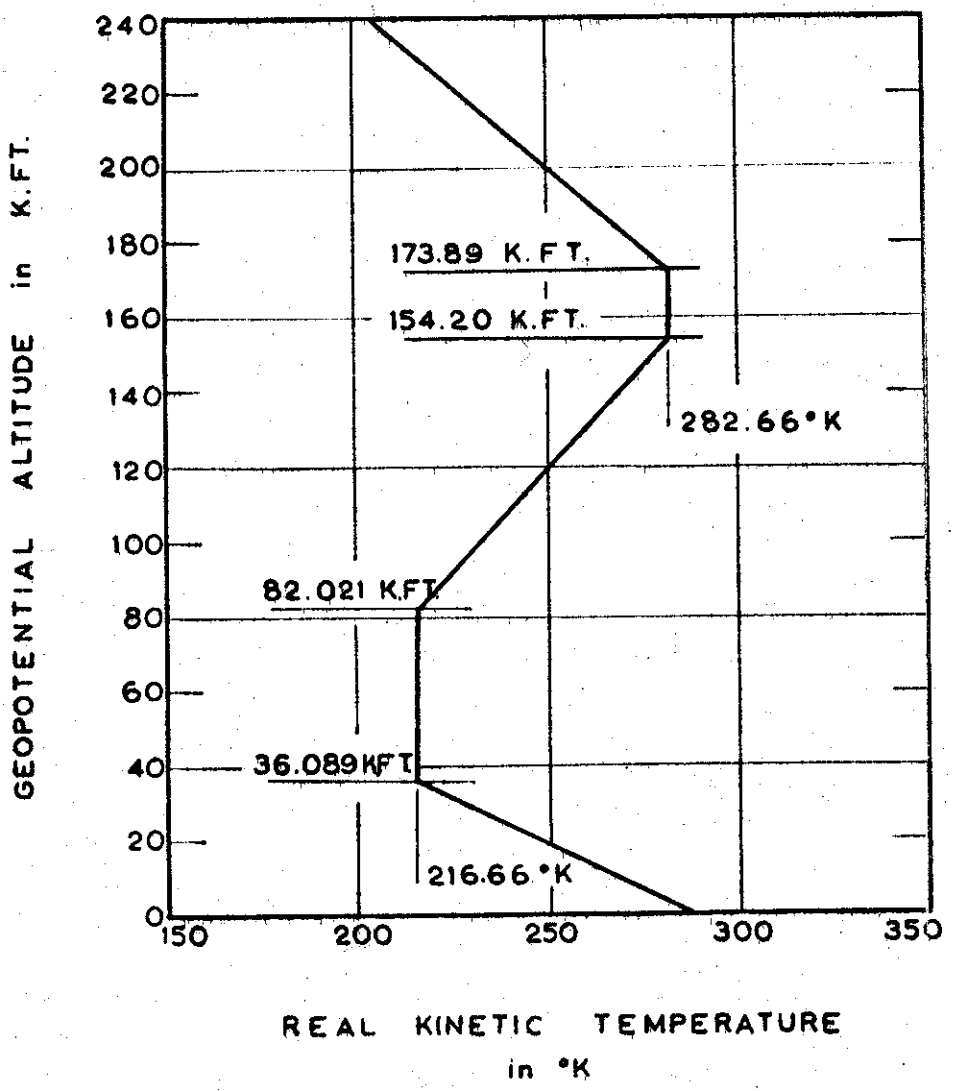

FIG. 6 ALTITUDE - TEMPERATURE CHART

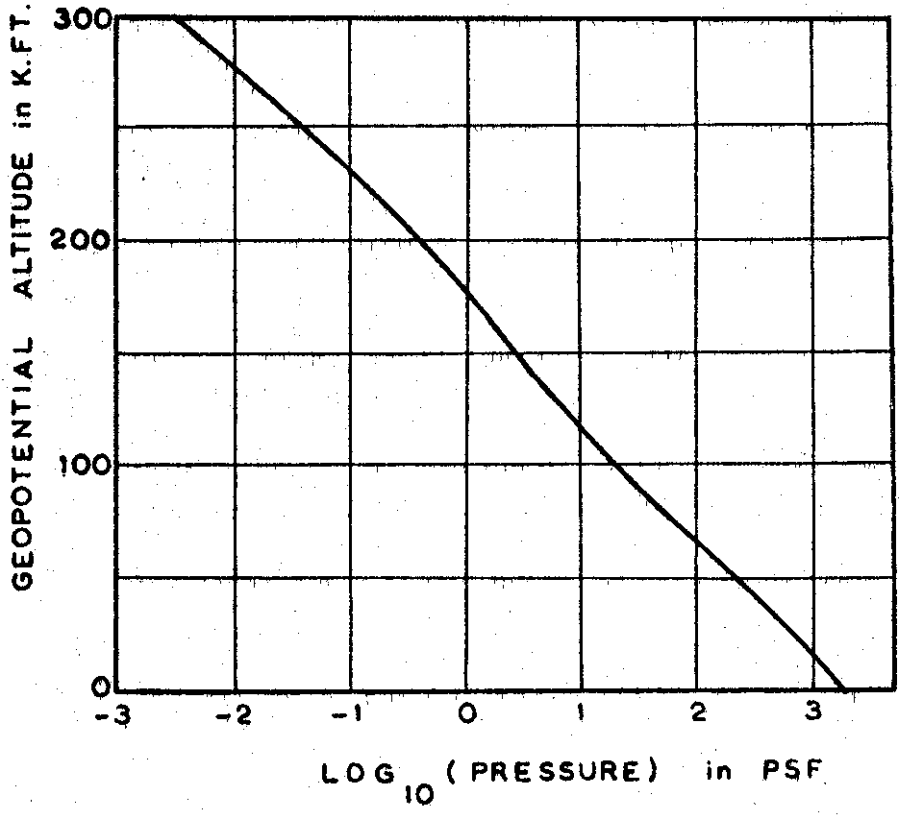

FIG. 7 ALTITUDE - PRESSURE CHARTS

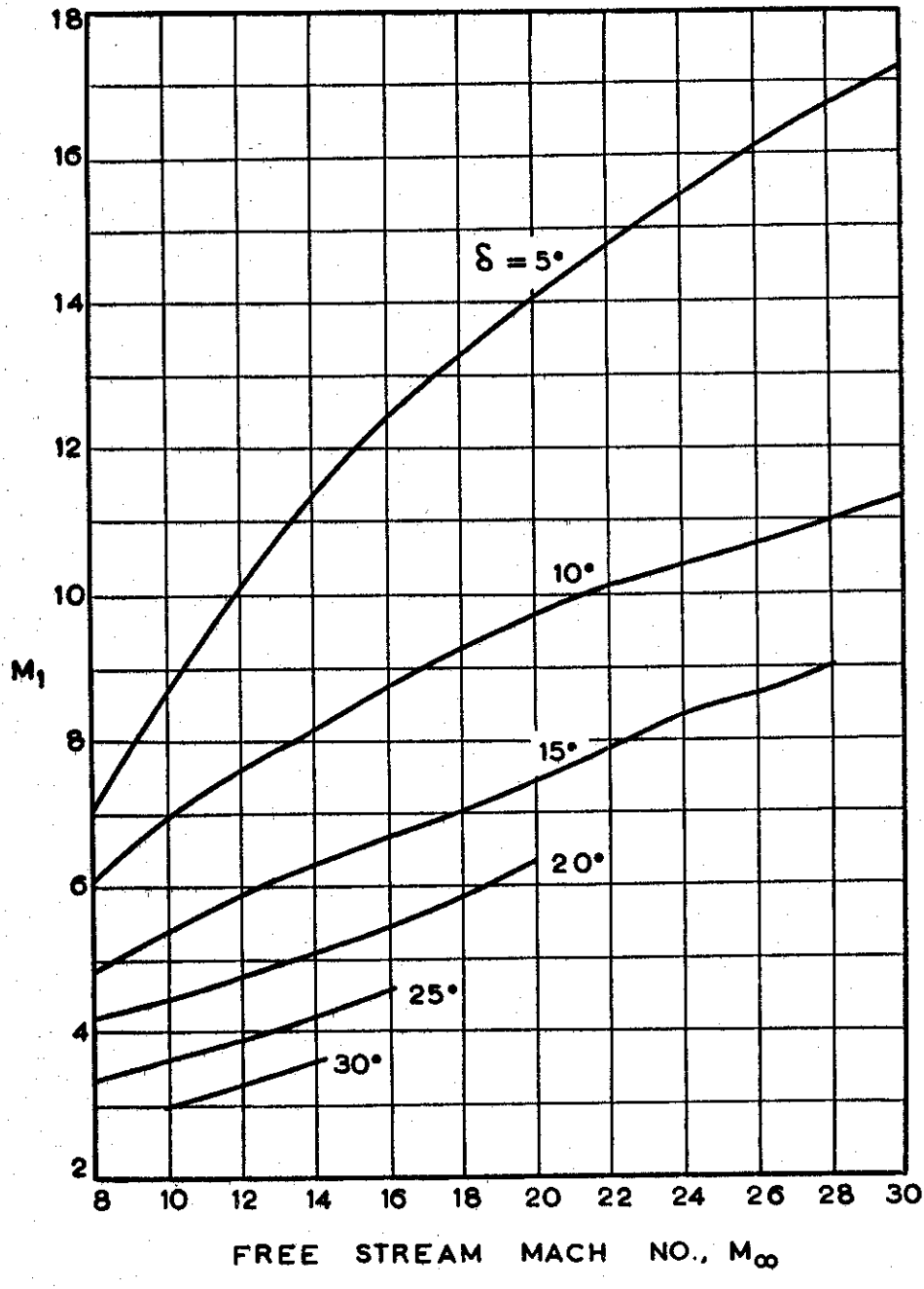

FIG. 8 MACH NUMBER AFTER FIRST SHOCKS VS. M_∞ AND δ FOR $\alpha = 0°$

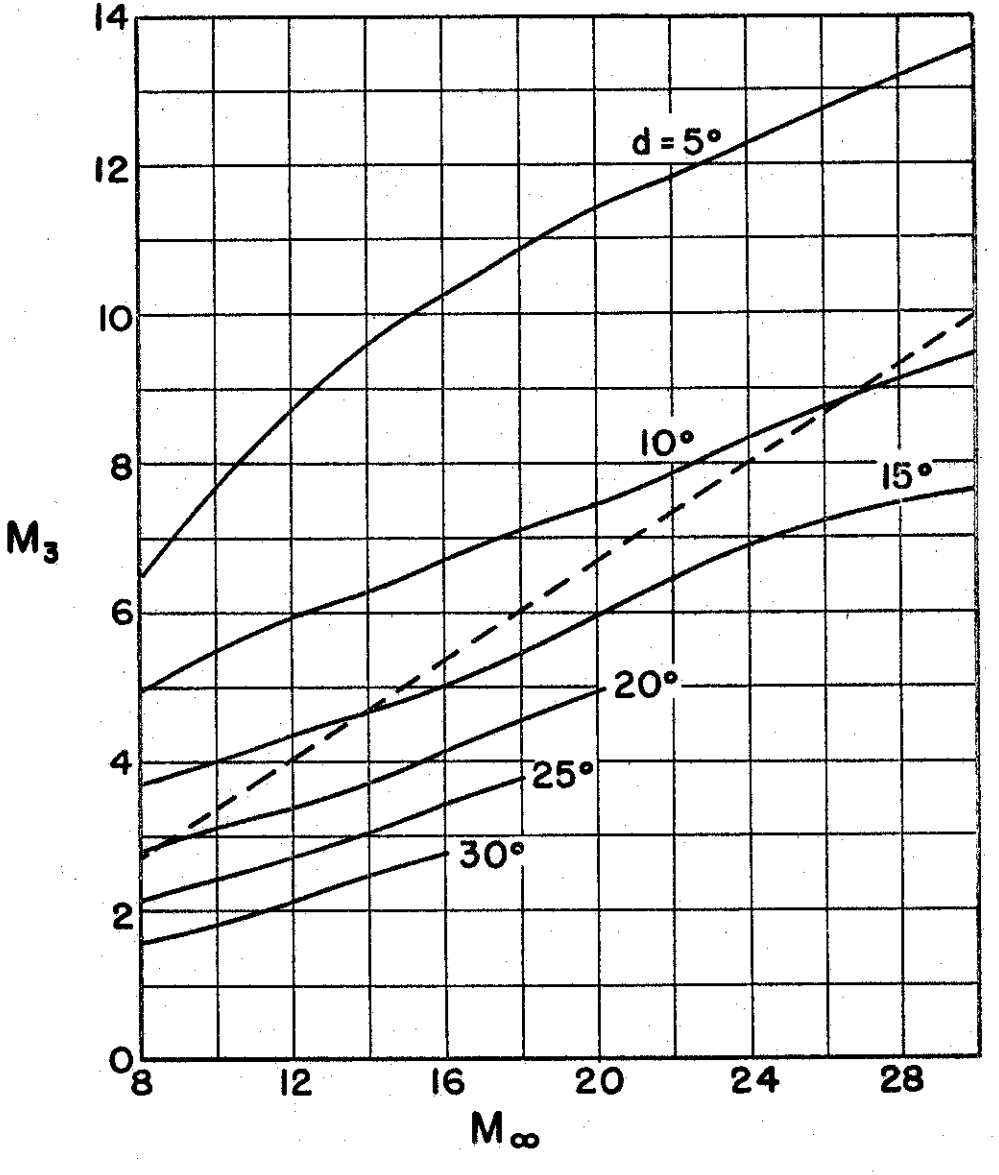

FIG. 9 MACH NUMBER AFTER INTERACTION VS. M_∞ AND d FOR $\alpha = 0°$

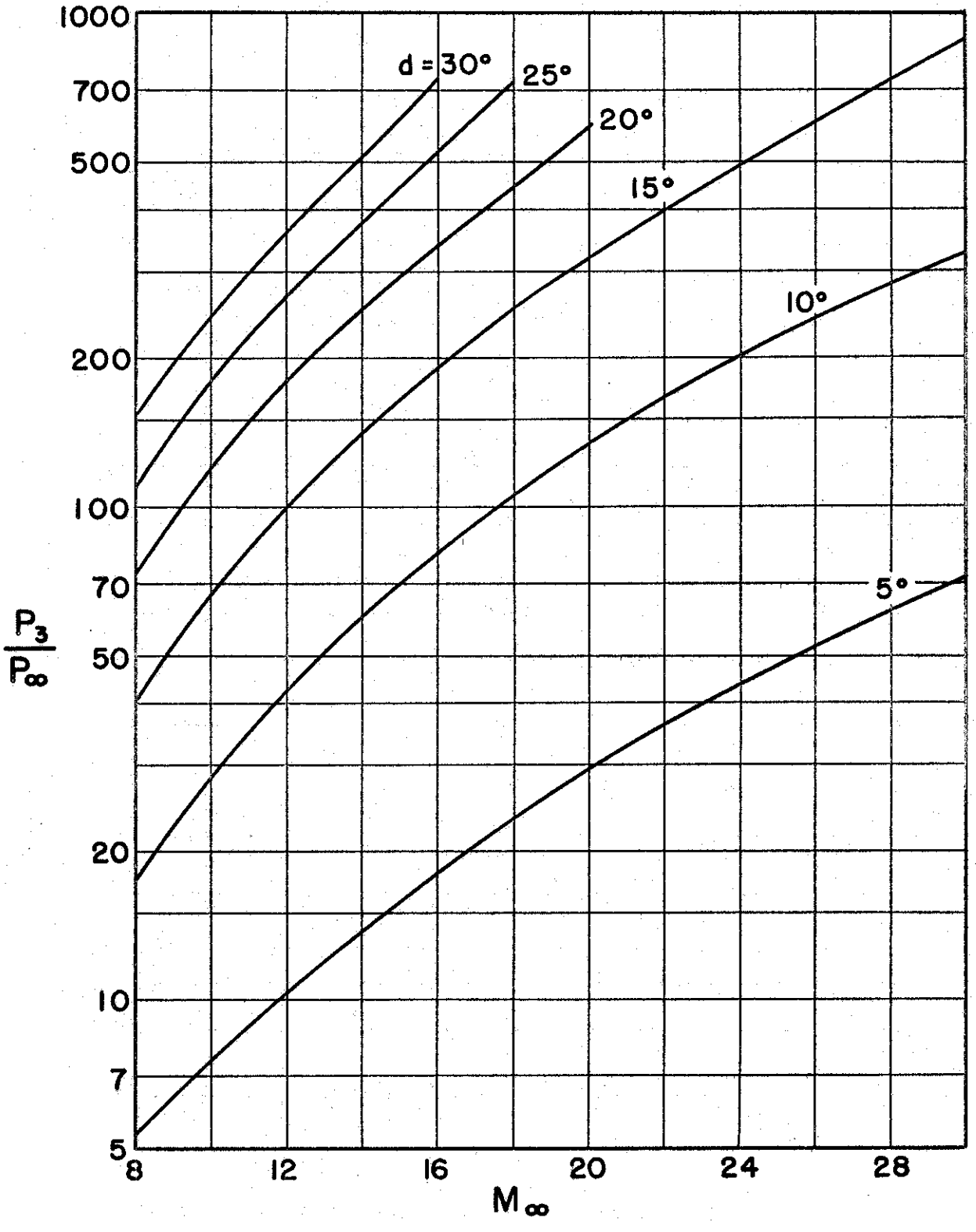

FIG. 10 PRESSURE RATIO P_3/P_∞ VS. M_∞ AND d FOR $\alpha = 0°$

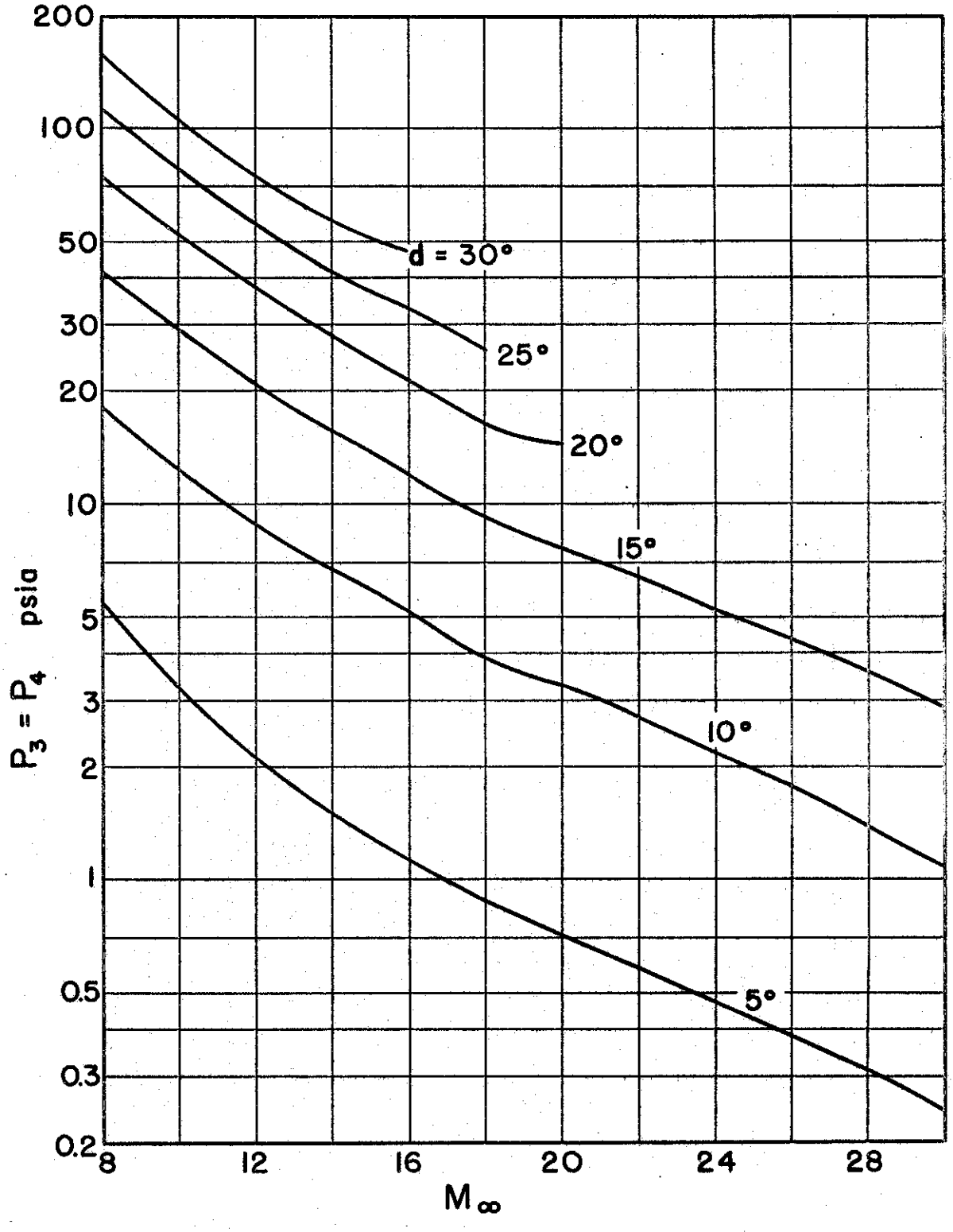

FIG. 11 PRESSURE P_3 VS. M_∞ AND d FOR $\alpha = 0°$

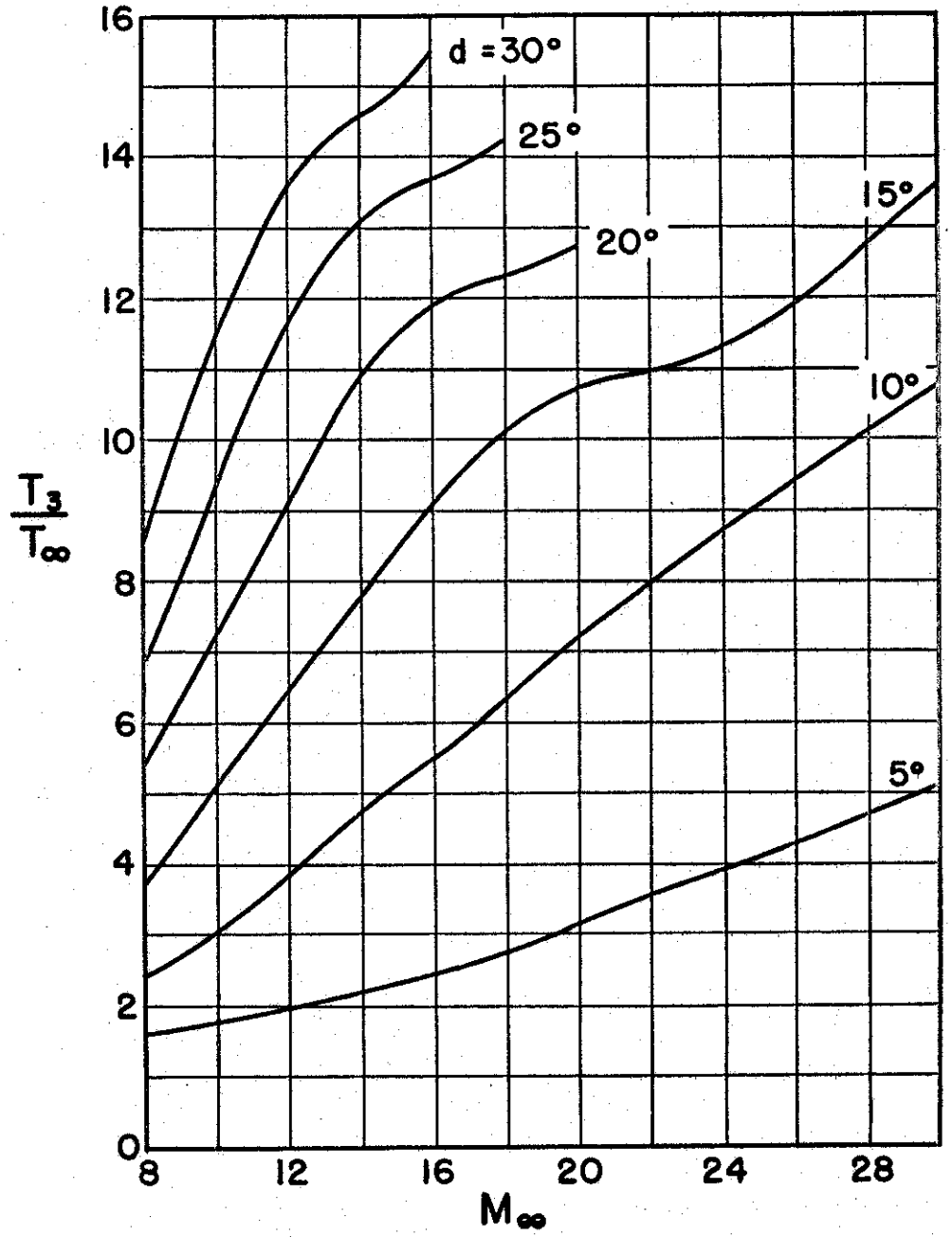

FIG. 12 TEMPERATURE RATIO T_3/T_∞ VS. M_∞ AND d FOR $\alpha = 0°$

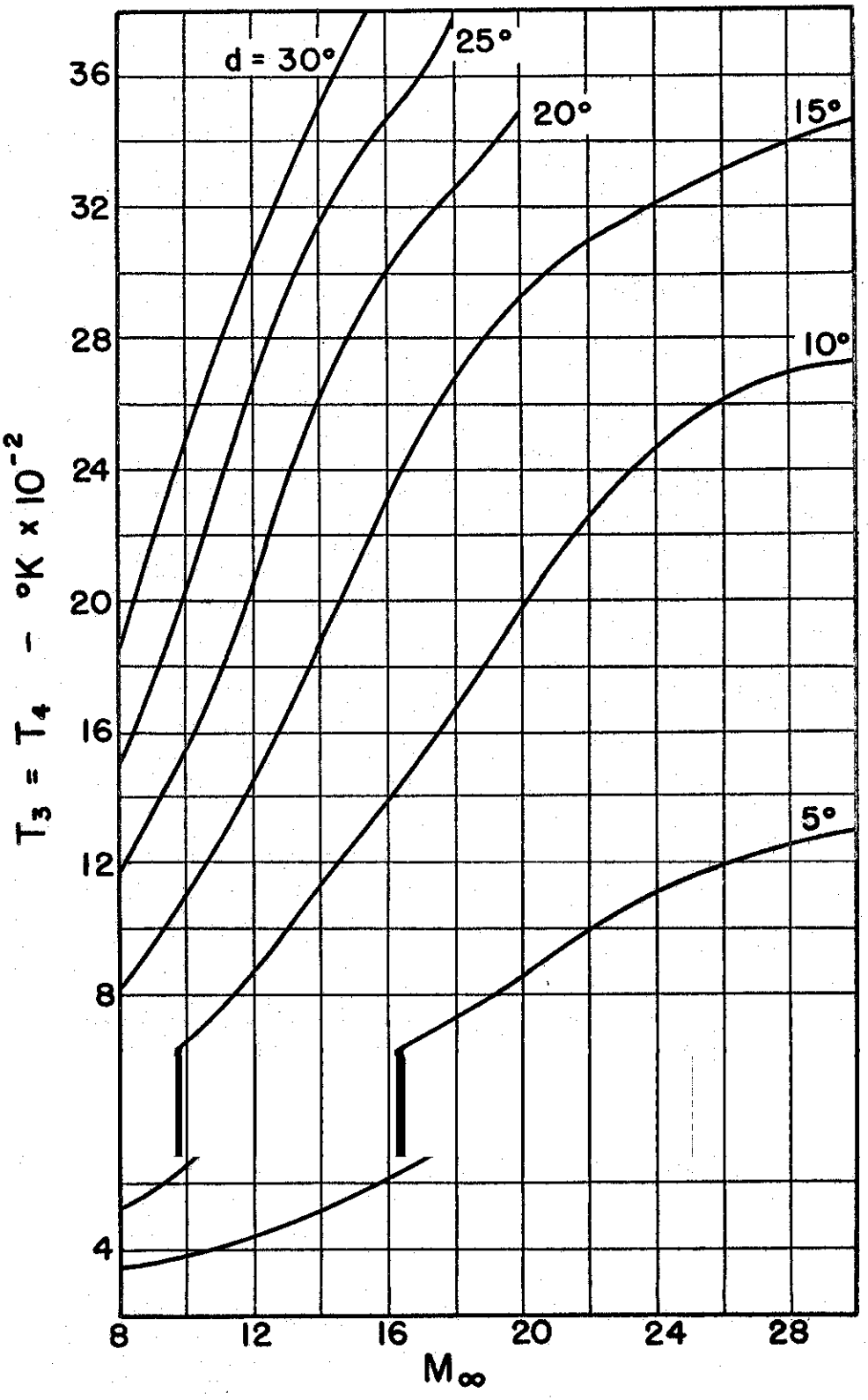

FIG. 13 TEMPERATURE T_- VS. M_∞ AND d FOR $\alpha = 0°$

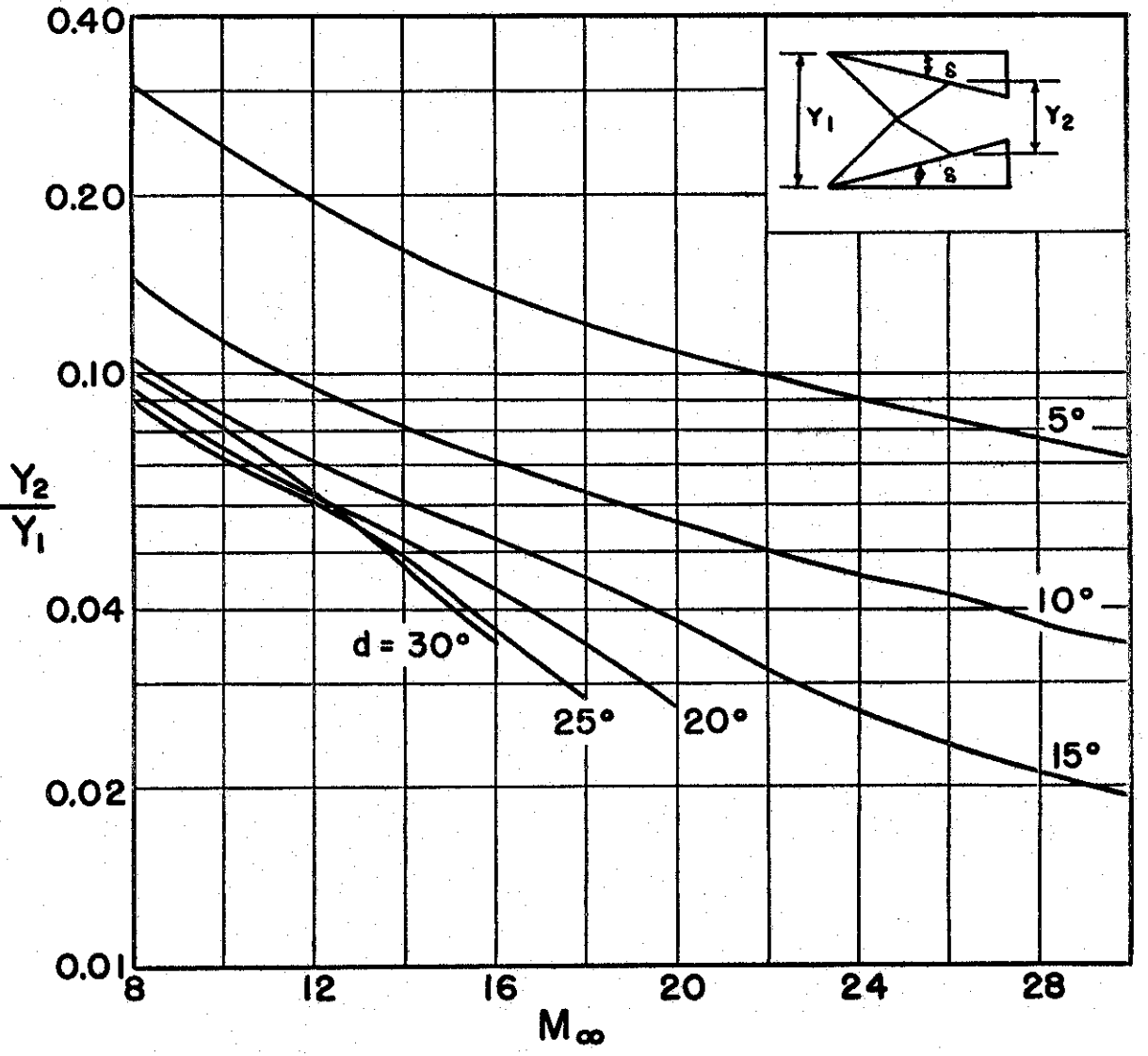

FIG. 14 AREA RATIO OR HEIGHT RATIO VS. M_∞ AND d FOR $\alpha = 0°$

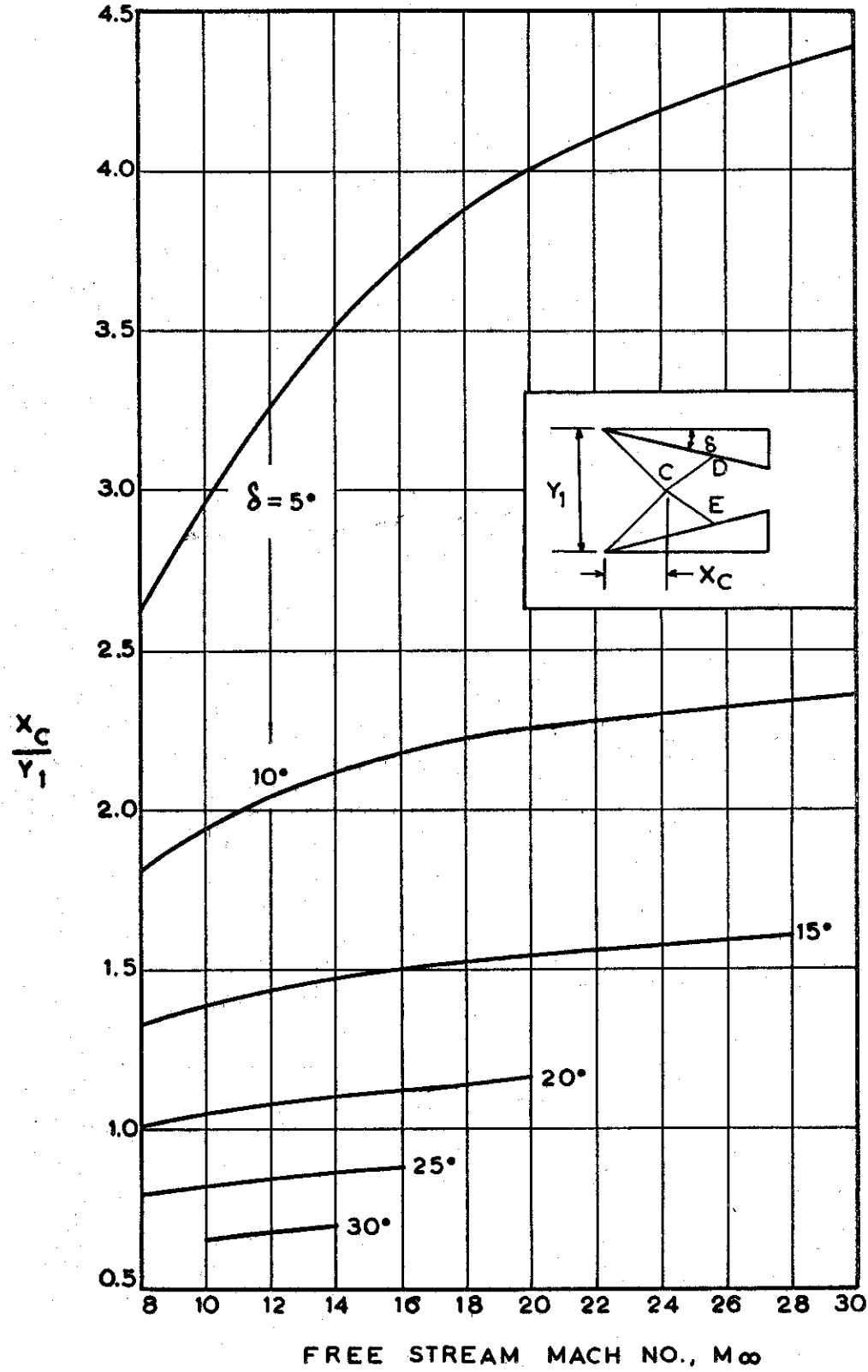

FIG. 15 RATIO OF DISTANCE OF POINT OF INTERACTION TO INTAKE HEIGHT VS. M_∞ AND δ FOR $\alpha = 0°$

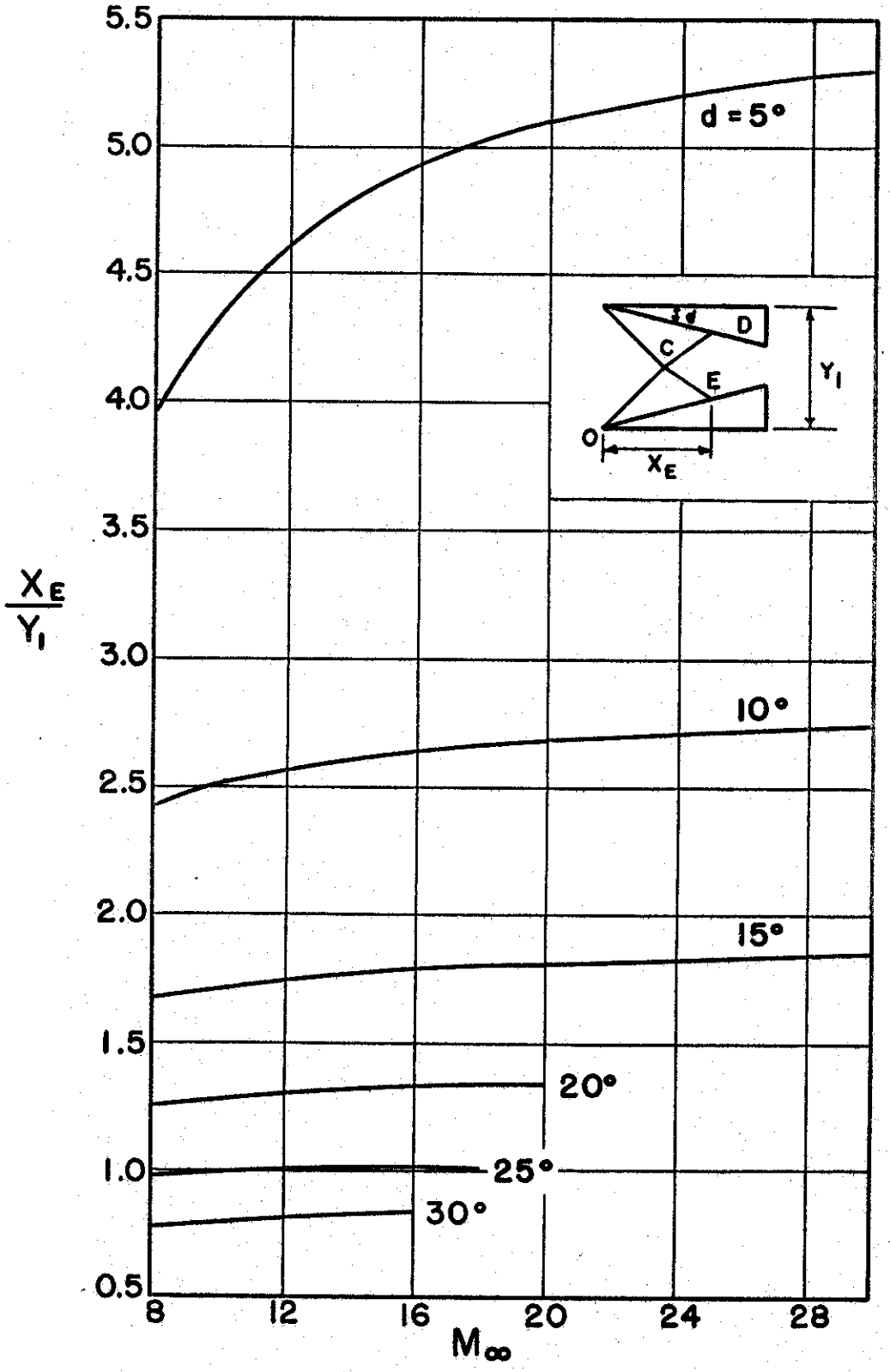

FIG. 16 INTAKE LENGTH TO HEIGHT RATIO VS. M_∞ AND d FOR $\alpha = 0°$

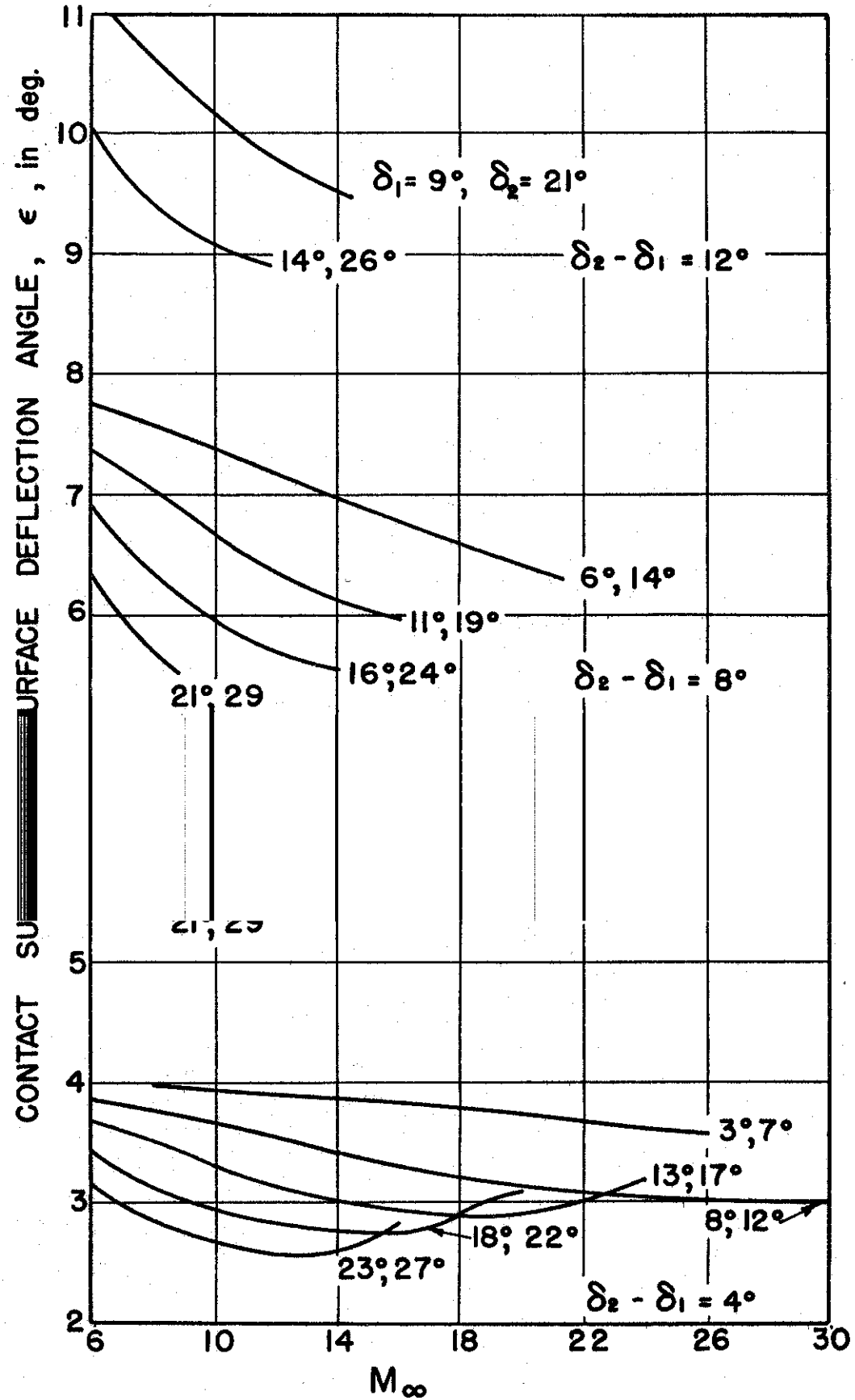
CONTACT SURFACE DEFLECTION ANGLE, ϵ, in deg.
11
10
9
8
7
6
5
4
3
2
6
10
14
18
22
26
30
M∞
δ1 = 9°, δ2 = 21°
14°, 26°
δ2 - δ1 = 12°
6°, 14°
11°, 19°
16°, 24°
δ2 - δ1 = 8°
21° 29
3°, 7°
13°, 17°
8°, 12°
18°, 22°
23°, 27°
δ2 - δ1 = 4°

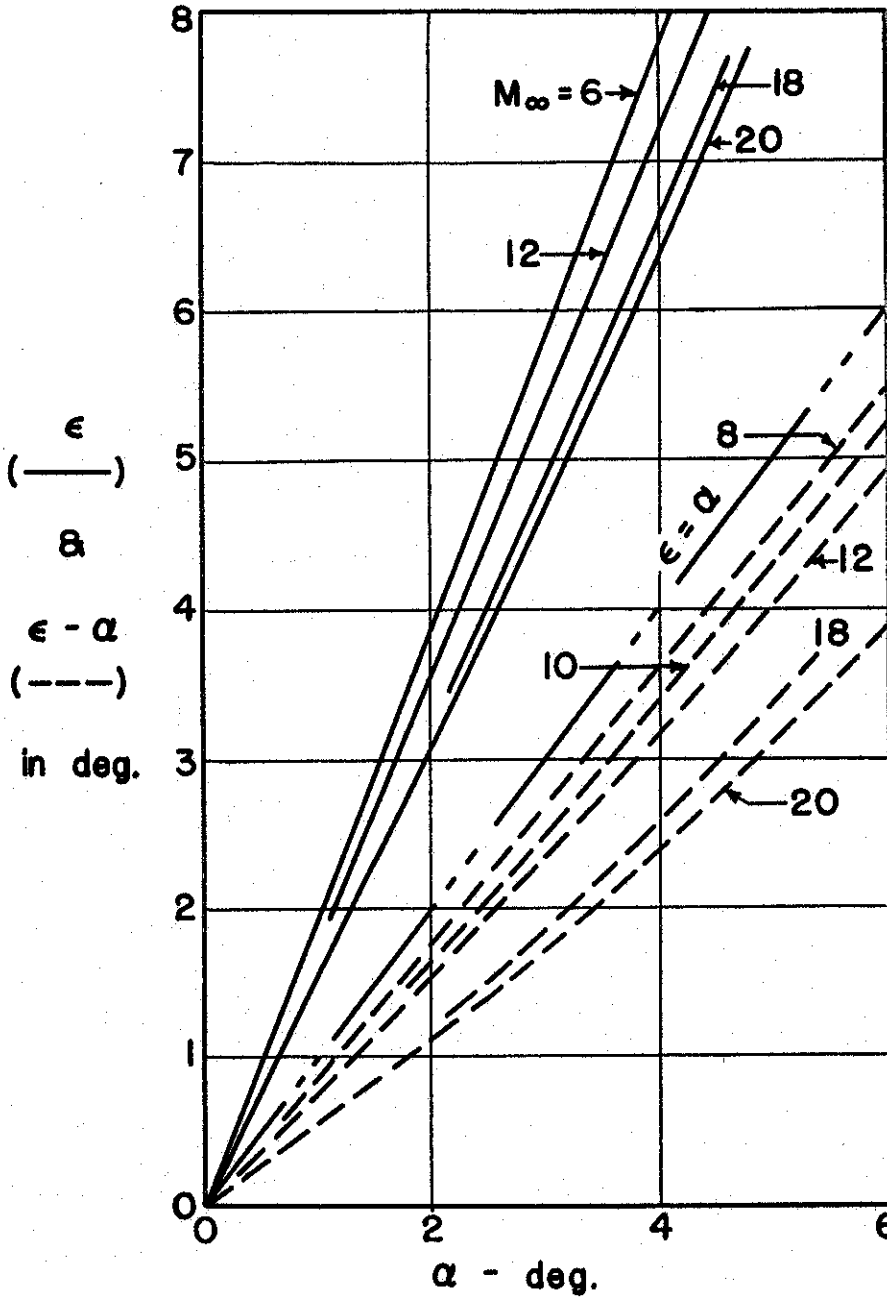

FIG. 18 VARIATION OF SLIPSTREAM DEFLECTION ANGLE WITH M_∞ AND α FOR d = 10°

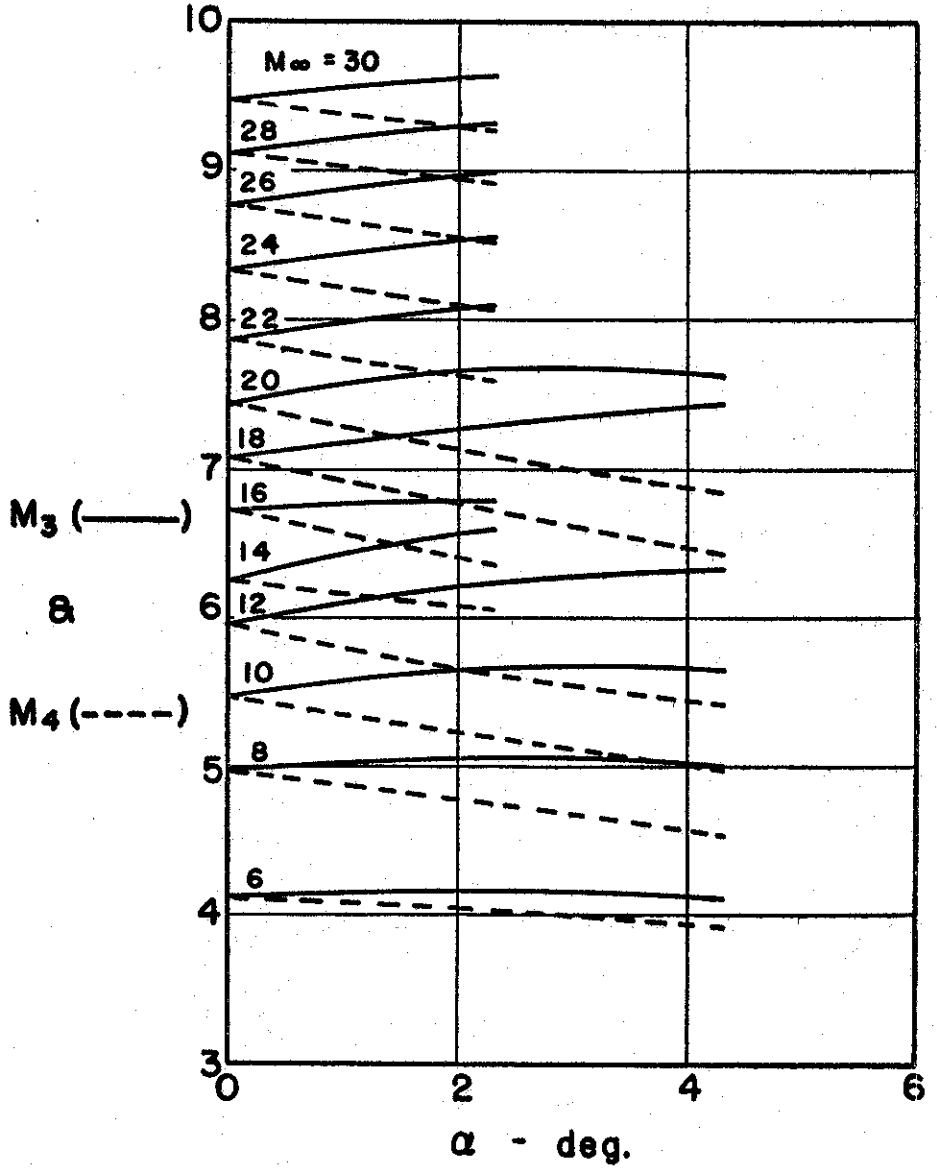

FIG. 19 VARIATION OF MACH NUMBERS AFTER SHOCK INTERACTION WITH M_{∞} AND α FOR d = 10°

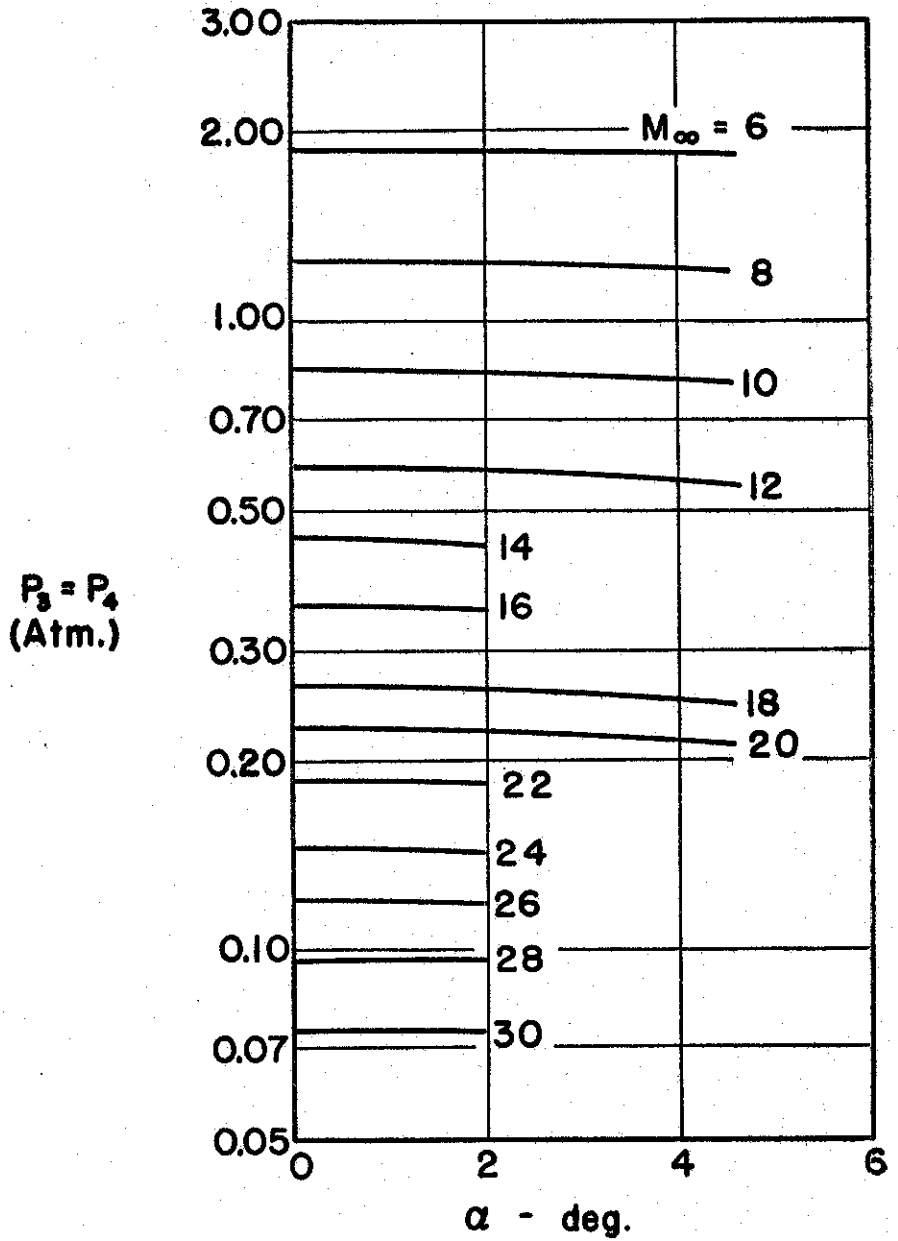

FIG. 20 PRESSURE AFTER SHOCK INTERACTION VS. α AND M_∞ FOR d = 10°

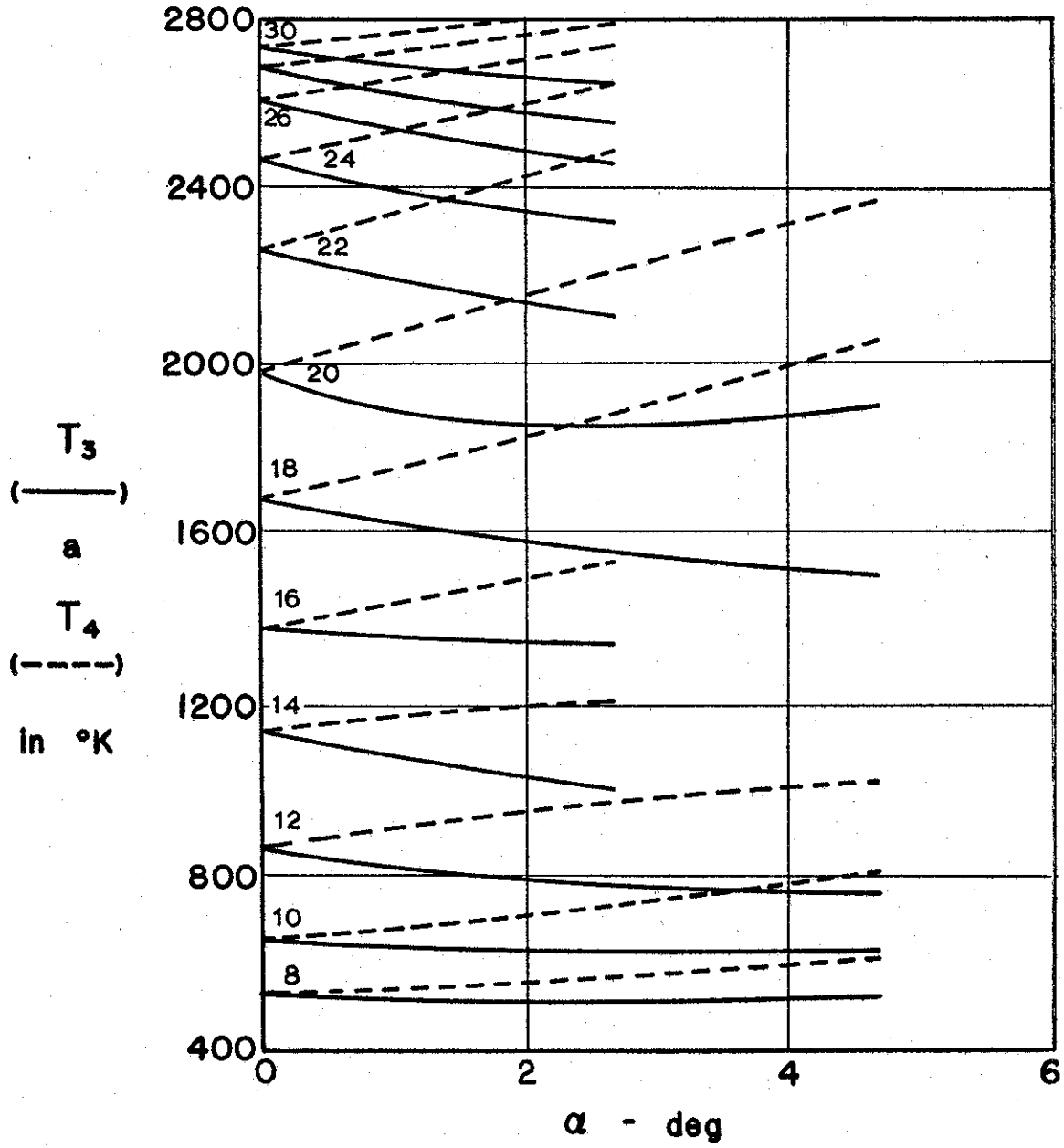

FIG. 21 TEMPERATURE AFTER SHOCK INTERACTION VS. α AND M_∞ FOR d = 10°

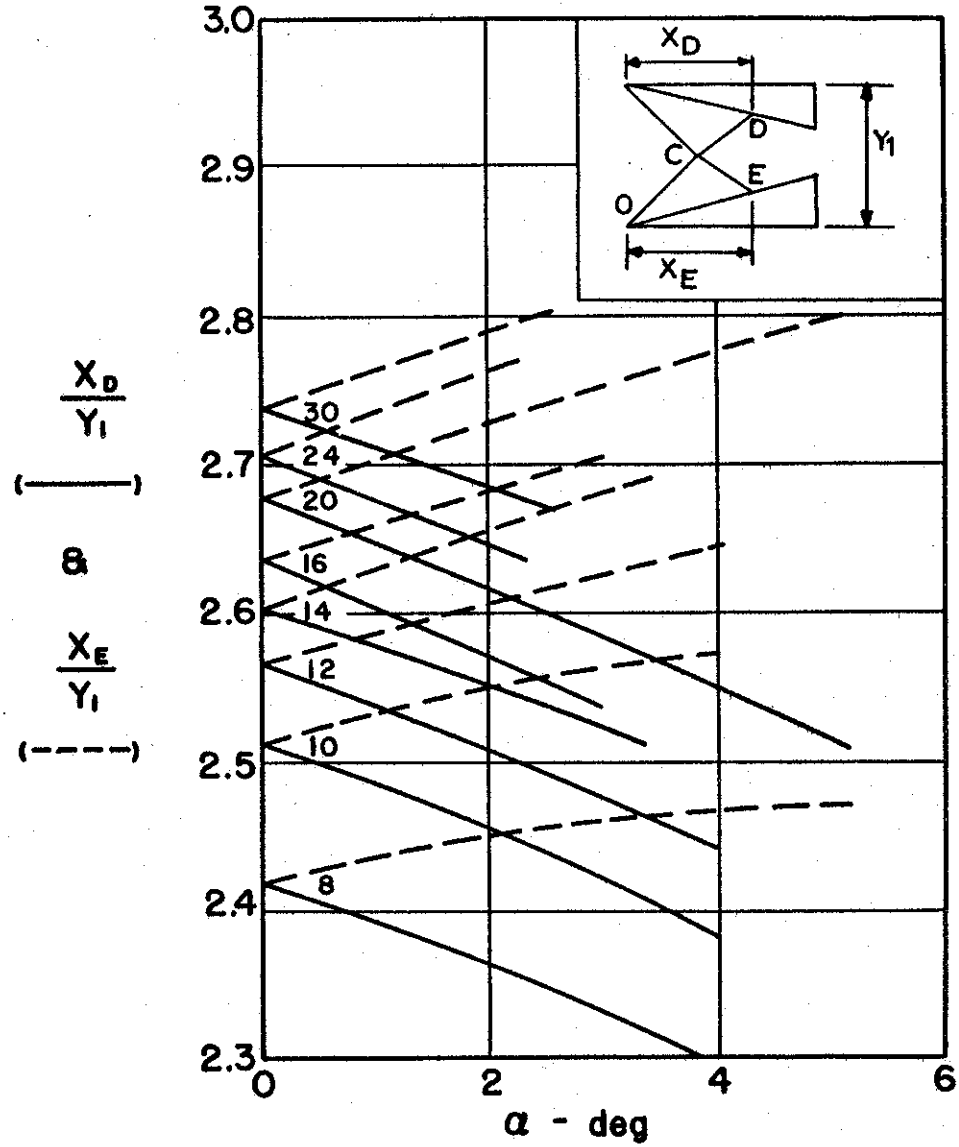

FIG. 22 X - CO-ORDINATES OF D AND E VS. α AND M_∞ FOR d = 10°

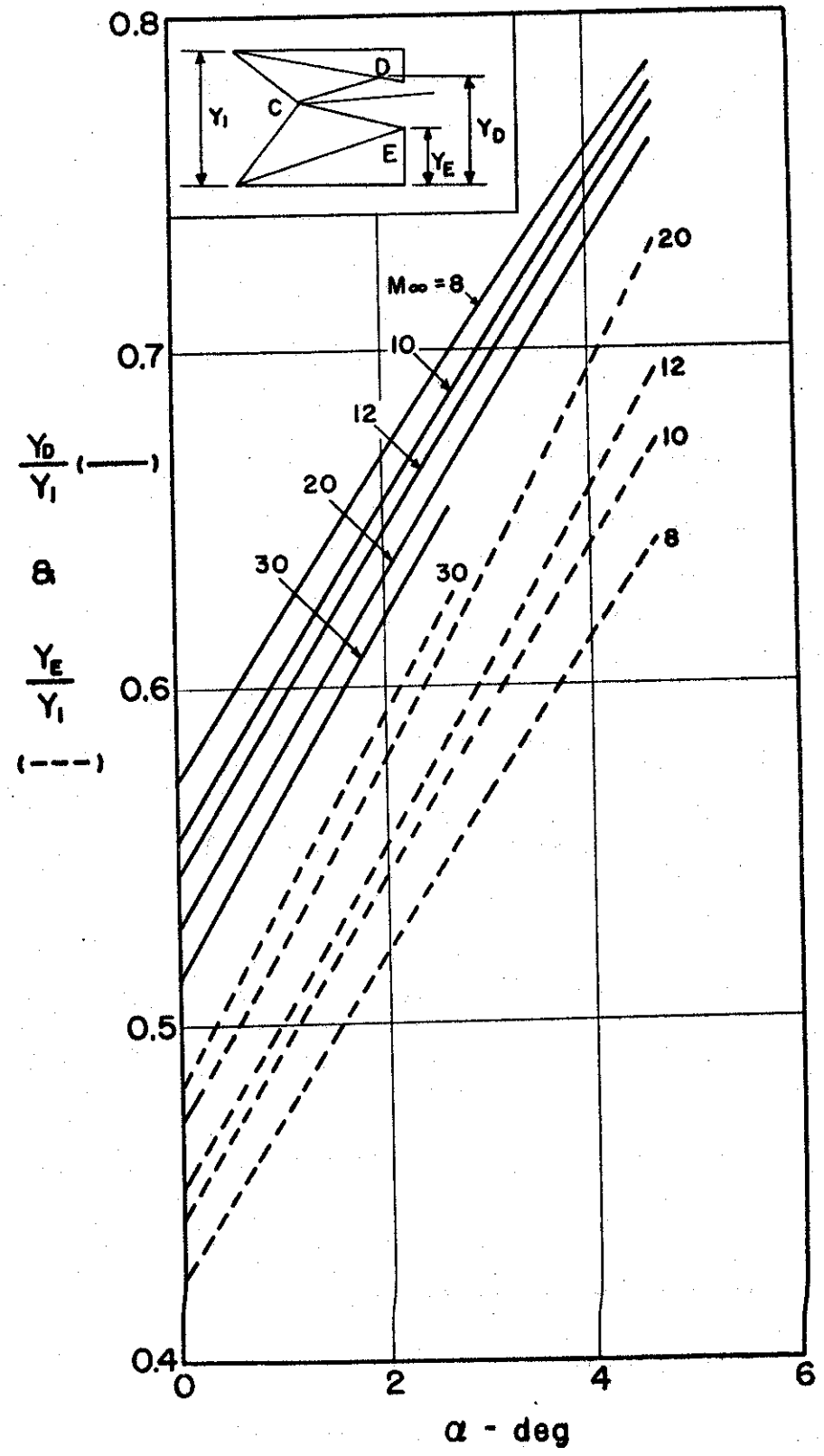

FIG. 23 Y - CO-ORDINATES OF D AND E VS. α AND M_∞ FOR d = 10°

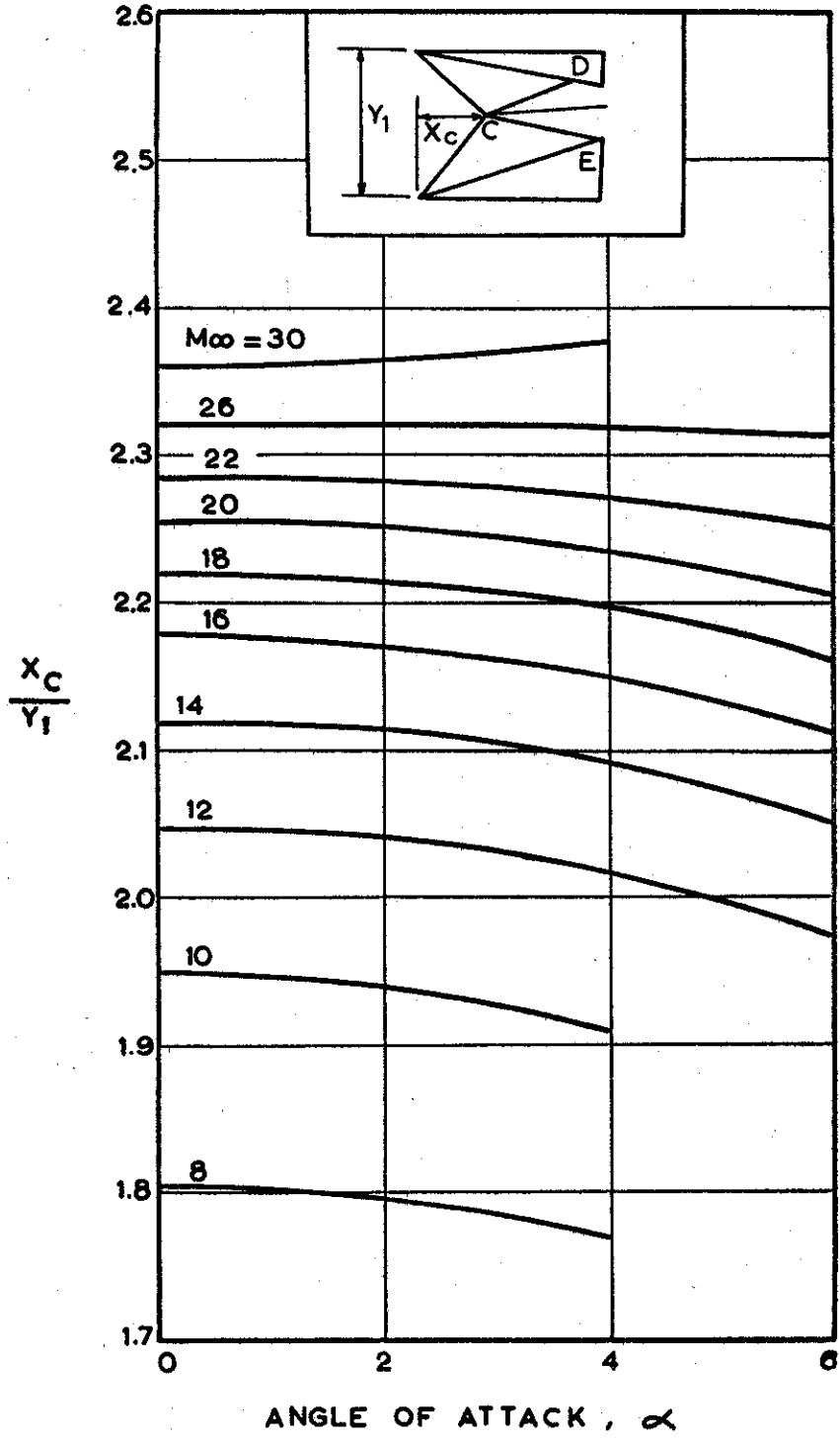

FIG. 24 X - CO-ORDINATE OF POINT OF INTERACTION VS. α AND M_∞ FOR d = 10°

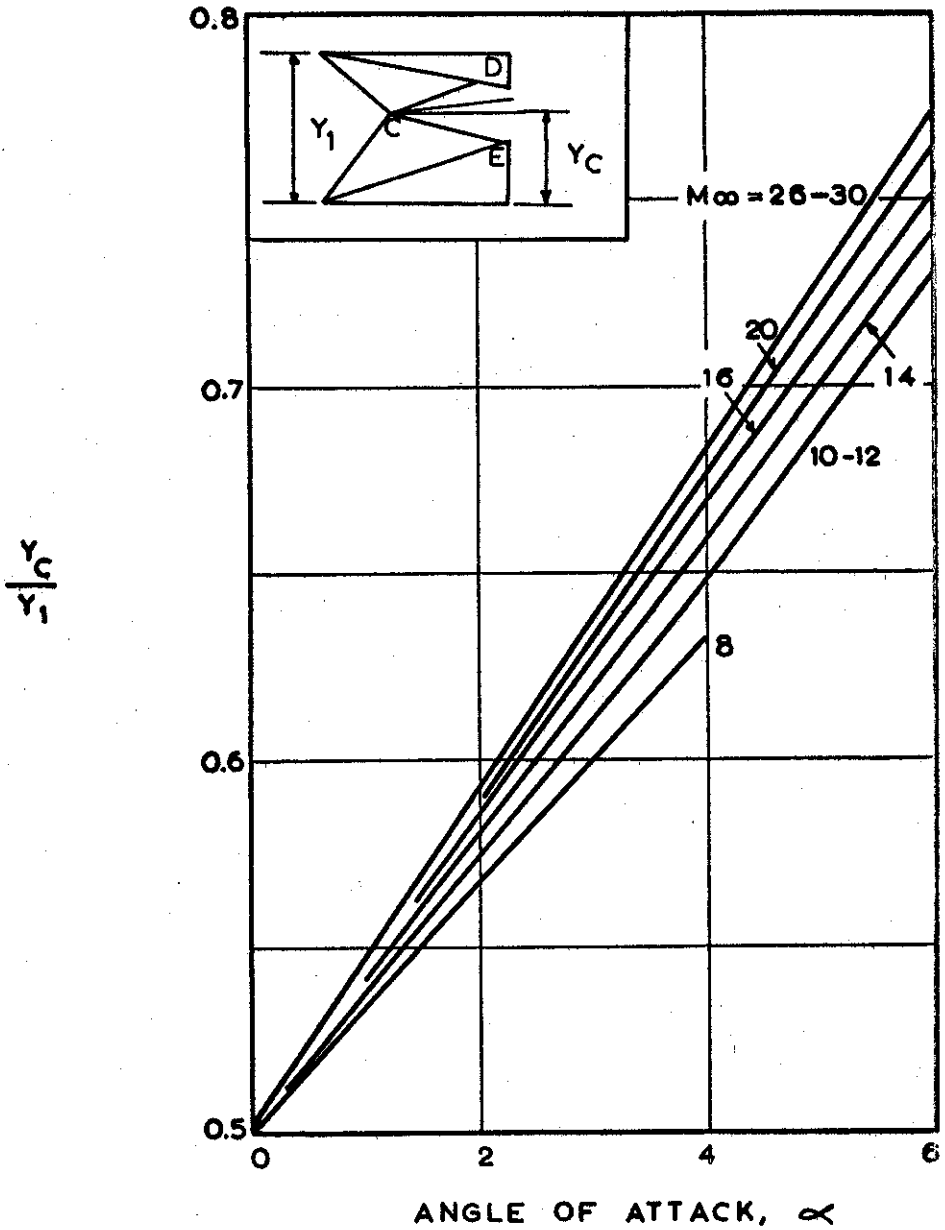

FIG. 25 Y - CO-ORDINATE OF POINT OF INTERACTION VS. α AND M_∞ FOR d = 10°

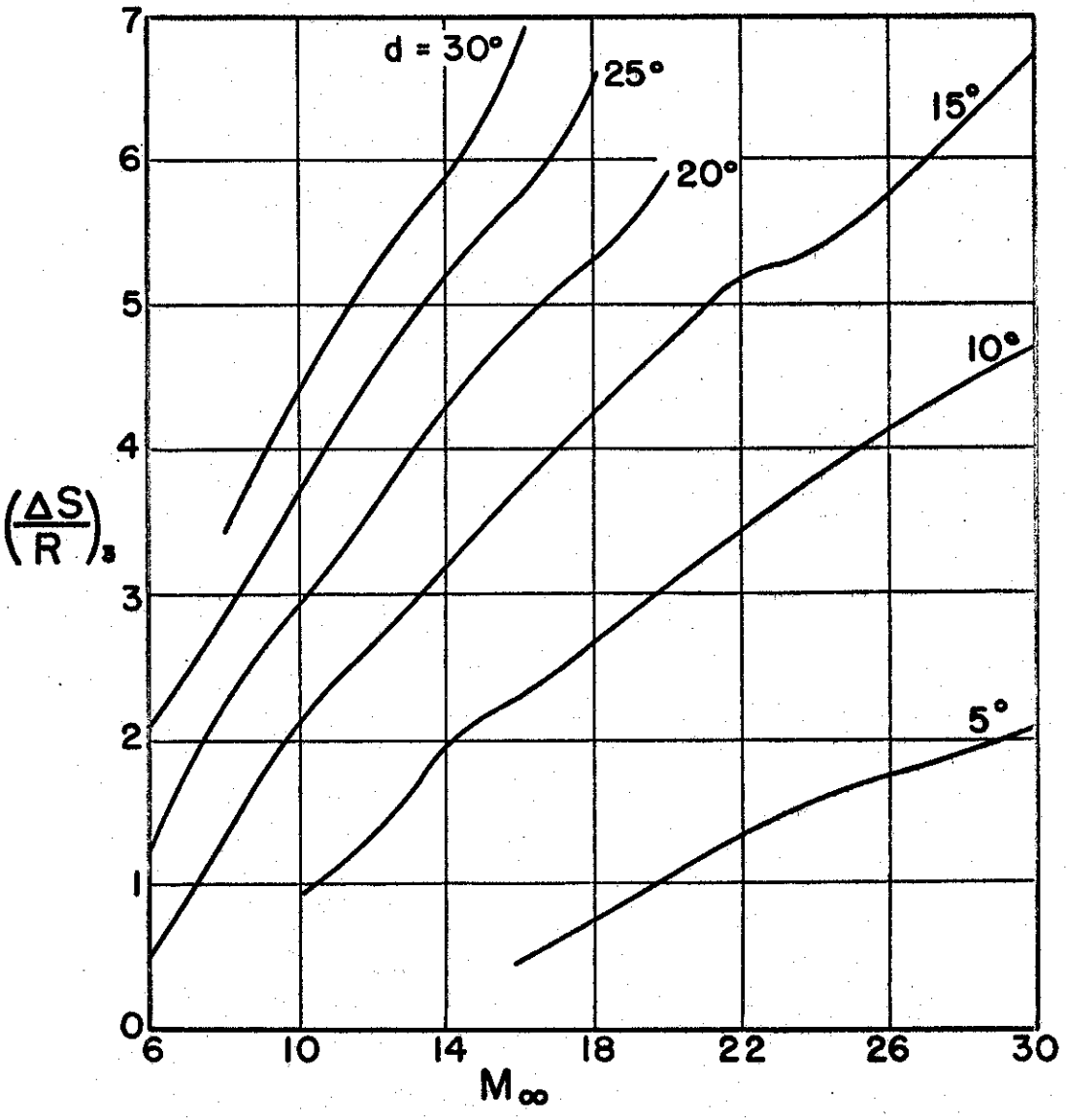

FIG. 26 ENTROPY INCREASE VS. M_∞ AND d FOR $\alpha = 0°$

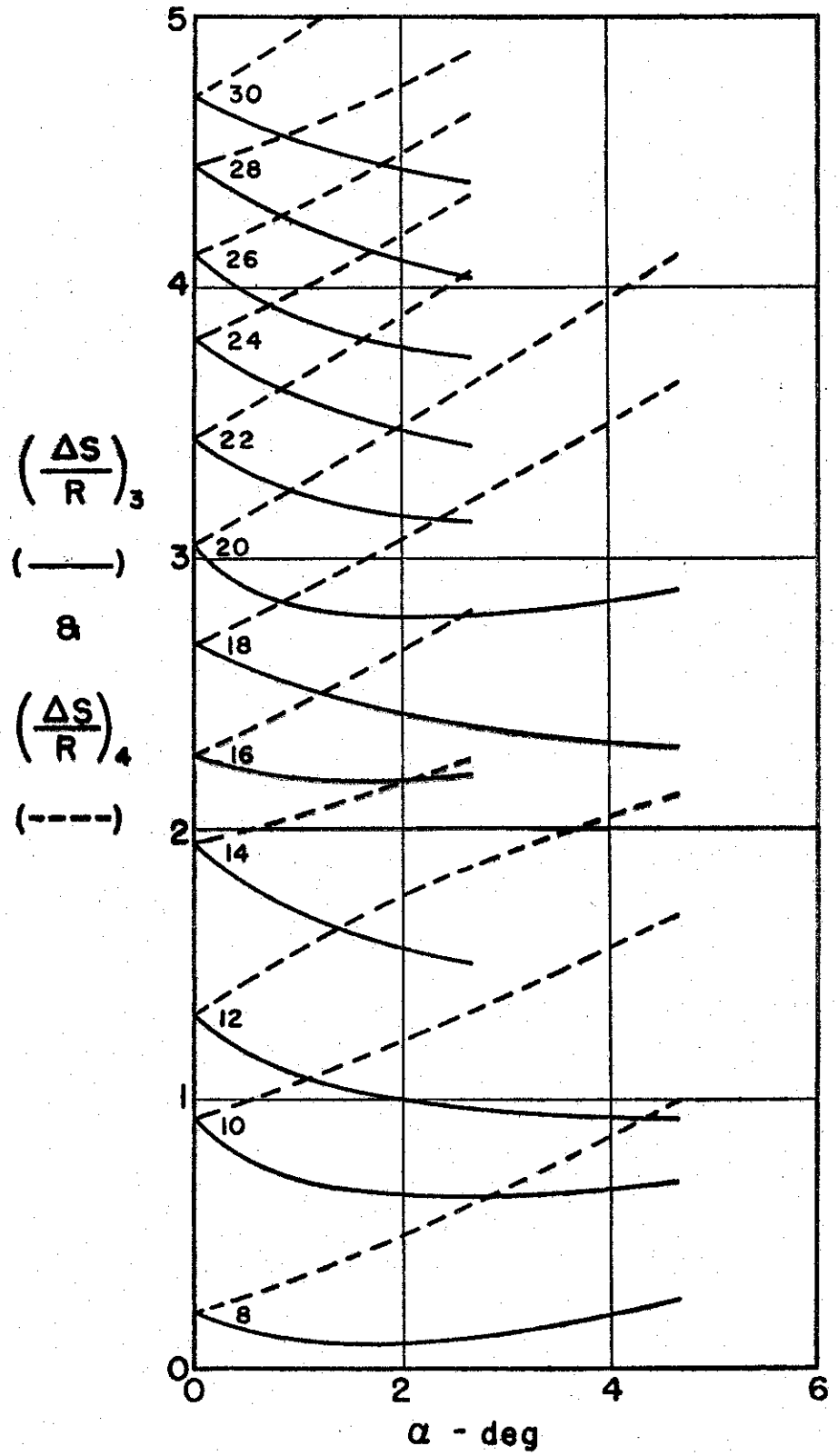

FIG. 27 ENTROPY INCREASE VS. α AND M_∞ FOR d = 10°

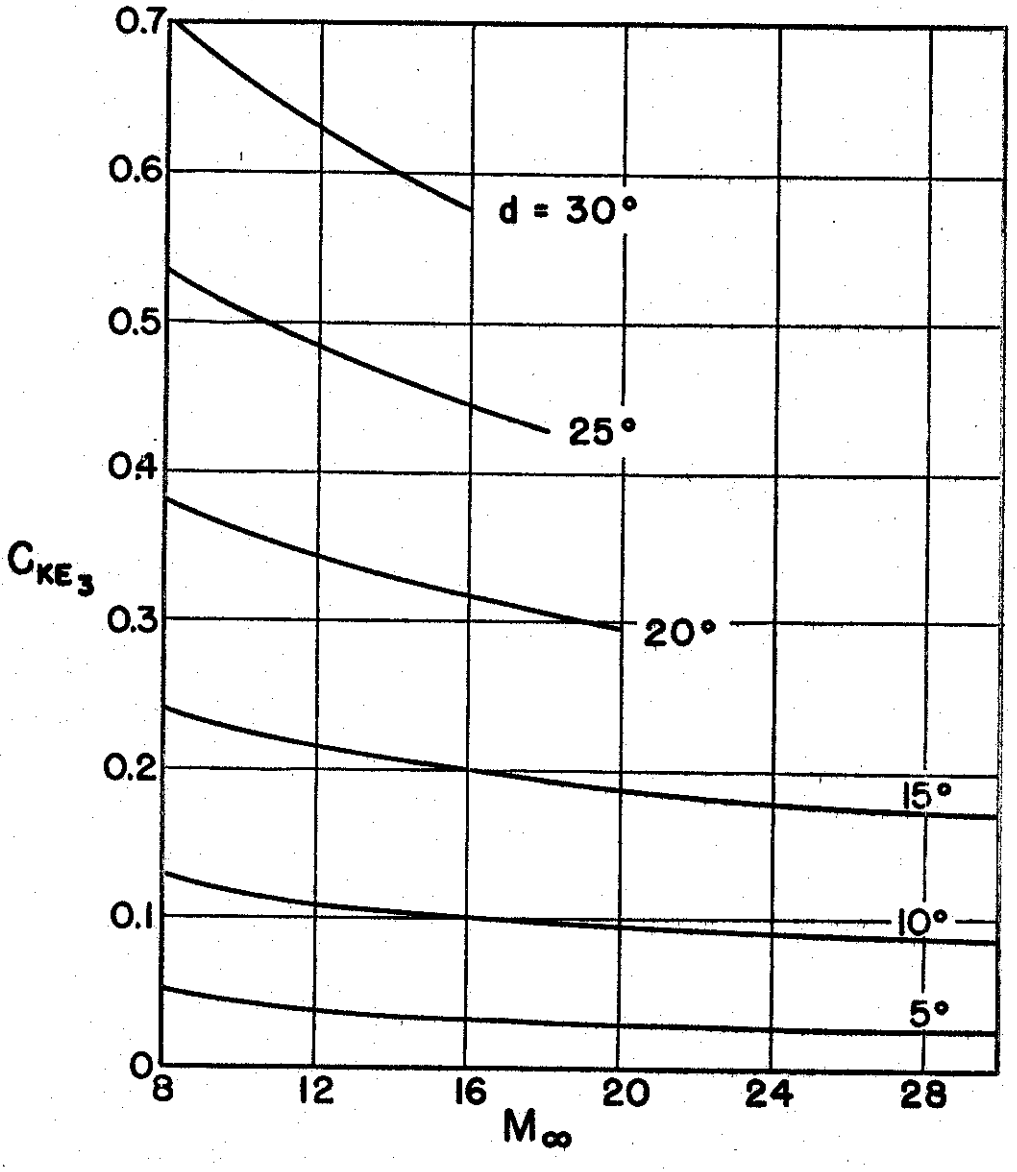

FIG. 28 KINETIC ENERGY COEFFICIENT (C_{KE}) VS. M_∞ AND d FOR $\alpha = 0°$

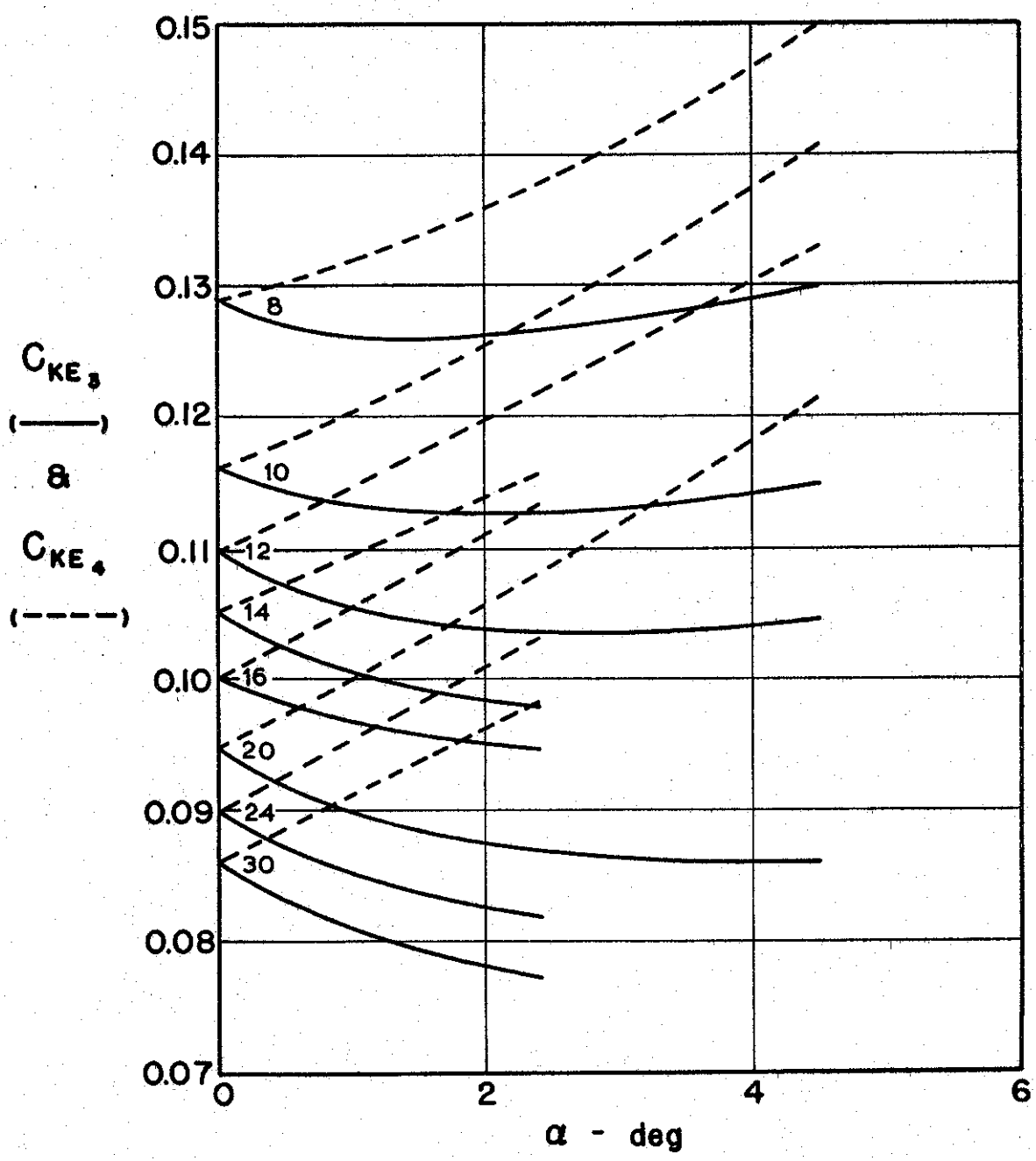

FIG. 29 KINETIC ENERGY COEFFICIENT VS. α AND M_∞ FOR d = 10°